Statistical Mechanical Modelling of Unstructured Proteins

Fermented Milk Casein Adsorption on Packaging Materials

charge regulation, polyelectrolyte-surface interactions, Monte Carlo simulations

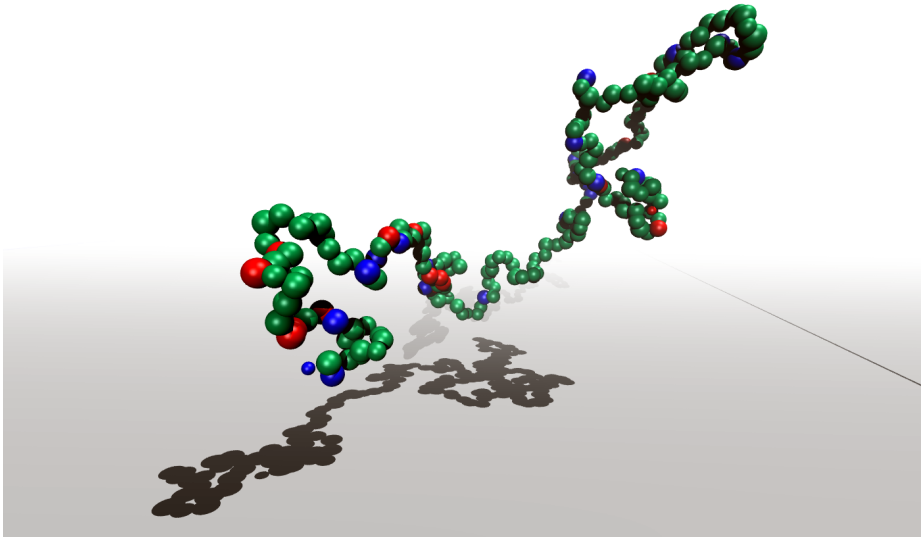

Chris H. J. Evers*

Supervisors:
Thorbjörn Andersson†
Mikael Lund*
Marie Skepö*

September 13, 2011

†Tetra Pak Packaging Solutions AB
*Theoretical Chemistry, Lund University

chris.evers@gmail.com
Master's thesis Organizing Molecular Matter

Department of Theoretical Chemistry
Chemical Center
Lund University
P.O. Box 124
S-221 00 Lund
Sweden

Front cover: Illustration of β-casein interacting with a negatively charged surface

Abstract

Caseins are the most abundant proteins in milk products and are thought to be crucial for many of its properties, like texture, viscosity, but also adhesion to packaging materials. The latter leads to a product loss of about 10%, and economical and environmental problems, and its molecular origin is here investigated from the interaction between β-casein and different surface materials. A theoretical zero model has been assembled, and a coarse grained model with implicit salt interactions is developed for Monte Carlo simulations. For small peptides, good agreement between the zero model and simulations is observed, but to investigate larger peptides simulations are necessary. These show that β-casein-surface adsorption is an interplay of electrostatic, hydrophobic, and charge regulation phenomena. Due to its amphiphilic properties and its high charge capacitance, β-casein acts as a molecular chameleon, adapting its charge to its environment and utilizing different adsorption mechanisms depending on the surface properties. Changing the surface parameters has therefore a clear effect on the adsorption mechanisms, but adsorption is nevertheless seen on most surfaces.

Chris H.J. Evers BSc.

Självfästande Filmjölk

Många upplever vid frukostbordet att det är bökigt och kladdigt att hälla ur *all* filmjölk ur paketet, så när konsumenten anser att förpackningen är tom finns det cirka 10% kvar av produkten. Detta är något som gemene man inte reflekterar över. Eftersom en del av filmjölken fäster på förpackningens insida så innebär det att det slängs mängder med förstaklassig mat, och att minst 130 tusen av EU:s kossor producerar mjölk i onödan. Svårtömda förpackningar medför alltså stora kostnader för konsumenten, negativ miljöpåverkan från produktionen av bortkastad mjölk, men även problem med återvinningen av förpackningsmaterial. I samarbete med Tetra Pak, världens ledande företag inom process- och förpackningslösningar för livsmedel, har en del av det molekylära ursprunget av detta problem undersökts.

Filmjölk är en komplex blandning som huvudsakligen består av vatten, fett, kolhydrater och mjölkproteiner. De senare verkar vara en viktig anledning till att filmjölk fäster på förpackningens insida. För att få en helhetsbild av varför filmjölk blir kvar i förpackningen, och för att så småningom kunna utveckla bättre förpackningar exempelvis genom ytmodfiering eller genom att använda ett annat material, är det väsentligt att förstå växelverkan mellan proteinmolekyler och förpackningens yta. Det är anledningen till att vi har utvecklat en modell där vi undersöker hur det mest koncentrerade proteinet, alltså *β-kasein*, växelverkar med ytor med olika egenskaper. Med hjälp av datorsimuleringar har vi studerat hur proteinet uppför sig i närheten av olika ytor som ska motsvara förpackningsytor.

Kasein adsorption på förpackningar

Resultat från datorsimuleringar visar att β-kasein fäster på många olika sorters ytor, främst därför att proteinet består av delar med olika egenskaper. Dessutom beter sig proteinet som en kameleont, det vill säga, det anpassar sina egenskaper till omgivningen.

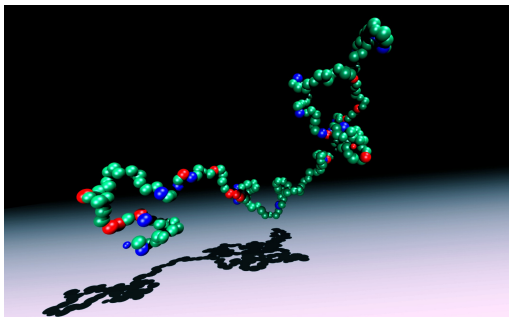

Filmjölks β-kasein häftar på förpackningsmaterial

Om β-kasein till exempel är i närheten av en yta med negativa laddningar, då blir vissa delar av proteinet mer positivt laddade. Positiva och negativa laddningar attraheras och de positiva delarna fastnar på ytan. Försöker man undvika det, genom att exempelvis byta ut de negativa ytladdningar mot positiva, så svarar proteinet med att bli mer negativt laddat, och fäster med den negativt laddade delen. Är ytan även *hydrofob*, alltså vattenskyende, då blir adsorptionen ännu starkare.

Resultaten i denna uppsats har gett oss en ökad insikt i hur β-kasein växelverkar och fäster på olika ytor. Vår förhoppning är att denna förståelse kan användas för att utveckla nytt icke-fästande förpackningsmaterial. På grund av filmjölkens komplexa natur som alla växelverkar olika med förpackningsytan så är utvecklingen av ett material som minskar vidhäftningen helt klart en stor utmaning.

Handledare: **Thorbjörn Andersson, Mikael Lund och Marie Skepö**
Examensarbete 30 hp i Organizing Molecular Matter, 2011-09-13
Teoretisk kemi, Lunds universitet
Tetra Pak Packaging Solutions

Chris H.J. Evers BSc.

Klevende yoghurt

Voor sommigen is het uitknijpen van yoghurtpakken een uitdaging; voor anderen is het een vervelend karwei, maar iedereen die denkt uiteindelijk alle yoghurt uit het pak te hebben geknepen, heeft gemiddeld bijna tien procent achtergelaten, doordat yoghurt aan het pak blijft kleven. Hier wordt meestal niet bij stil gestaan, maar een tiende deel hoogwaardige yoghurt wordt dus met het pak weggegooid. In de EU komt deze hoeveelheid overeen met de productie van 130 duizend koeien, die dus overbodige melk produceren. De productie en verwerking van deze weg te gooien yoghurt zorgt voor extra kosten voor consumenten, een grotere negatieve impact op het milieu en ook problemen bij de recycling van verpakkingsmateriaal. In samenwerking met Tetra Pak, 's werelds marktleider in processing- en verpakkingsconcepten voor levensmiddelen, is de moleculaire achtergrond van dit probleem onderzocht.

Melkproducten zijn een complex mengsel van hoofdzakelijk water, vet, koolhydraten en melkeiwitten. Die laatste lijken een belangrijke oorzaak te zijn voor het feit dat yoghurt aan de binnenkant van pakken blijft zitten. Om te begrijpen *waarom* yoghurt achterblijft, en om uiteindelijk betere pakken te ontwikkelen, bijvoorbeeld door oppervlaktebehandeling of door andere materialen te gebruiken, is het belangrijk de interacties tussen deze eiwitmoleculen en verpakkingsmateriaal in kaart te brengen. Daarom hebben we een model ontwikkeld voor het meest voorkomende eiwit, *β-caseïne*, en verpakkingsmaterialen met verschillende eigenschappen. Met behulp van computersimulaties is vervolgens het gedrag van het eiwit in de buurt van deze materialen onderzocht.

Caseïne adsorptie op verpakkingen

De computersimulaties laten zien dat β-caseïne op veel verschillende soorten materialen blijft kleven, omdat het ewit bestaat uit delen met verschillende eigenschappen. Bovendien gedraagt het molecuul zich als een kameleon; het past zijn eigenschappen namelijk aan zijn omgeving aan.

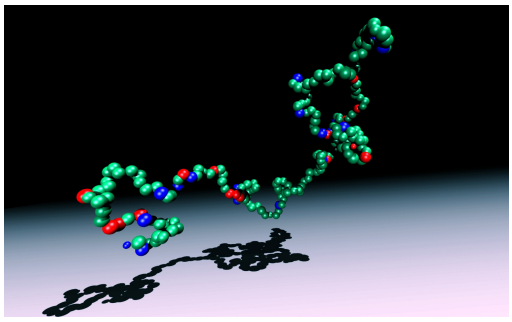

β-caseïne in yoghurt kleeft aan verpakkingsmateriaal

In de buurt van een negatief geladen oppervlak bijvoorbeeld worden bepaalde delen van β-caseïne meer positief geladen. Positieve en negatieve ladingen trekken elkaar aan en de positief geladen delen blijven aan het oppervlak kleven. Als je dit probeert te voorkomen door de negatieve oppervlakteladingen te vervangen door positieve, dan wordt het eiwit meer negatief geladen en blijven de negatief geladen delen plakken. Is het oppervlak daarnaast ook *hydrofoob*, dus waterafstotend, dan is de aantrekking nog sterker.

Het resultaat van dit onderzoek leidt tot een beter inzicht in hoe β-caseïne met een oppervlak wisselwerkt en blijft kleven op verschillende materialen. Dit begrip kan gebruikt worden bij de ontwikkeling van nieuw, niet-klevend verpakkingsmateriaal. Door de complexe natuur van yoghurt en β-caseïne zijn er echter vele verschillende manieren waarop yoghurt kan blijven plakken en is de ontwikkeling van een pak waar helemaal geen yoghurt in achterblijft een grote uitdaging.

Begeleiders: **Thorbjörn Andersson, Mikael Lund och Marie Skepö**
Masterthesis 30 ECTS in Organizing Molecular Matter, 2011-09-13
Theoretische chemie, Lund Universiteit
Tetra Pak Packaging Solutions AB, Lund

Contents

Chapter 1

Introduction

1.1 Fermented milk products

Fermented (or acidified) milk products, such as yoghurt and filmjölk in Scandinavia, have been produced for millennia by adding lactic acid bacteria to cow milk. These bacteria have a strong influence on two of the characteristic components in milk: lactose (milk sugar) and casein (a protein).

The bacteria convert lactose into lactic acid, leading to a reduction of the pH. This pH reduction causes the initially charged casein proteins which are aggregated in micelles to be titrated. The charge of the proteins increases, and the micelles partly dissociate and near pH 4.6-4.8 the milk flocculates. [1, 2, 3] The result is a viscous gel with the characteristic sour yoghurt taste.

Over the last ten years, the production of fermented milk products has risen in Europe, see Figure 1.1 (left). Many of these products are packed in carton packages, see Figure 1.1 (right), but when pouring out the milk, about 10% of the products is left in the package.

In 1999 the average milk production per cow was 5.7 tonne in the 15 countries[1] for which Eurostat data was available [4]. Assuming one litre cow milk gives one litre fermented milk, the number of cows producing milk only to be thrown away with the package is thus about 130 - 160 thousand for the time period of Figure 1.1 (left).

This leads to economic losses, and the production and processing of this non-consumed milk also gives unnecessary negative environmental impact. Furthermore, residual products in the packages give problems with the recycling of package material, and it can be considered unethical to throw 10% of edible food away, while hunger is still a problem in many parts of the world.

The main components of fermented milk are water, sugars, lactic acid, fat, salt and proteins. The ionic strength is 80 mM, and the two main protein types in milk are whey proteins (20%) and casein (80%), of which casein forms micelles which bind calcium phosphate for the neonate. [2, 5, 6]

In a simultaneously performed experimental study at Tetra Pak, it has been shown that proteins play a key role in the adsorption of fermented milk. [7] The

[1] Belgium, Denmark, Germany, Ireland, Greece, Spain, France, Italy, Luxembourg, the Netherlands, Austria, Portugal, Finland, Sweden, and the United Kingdom

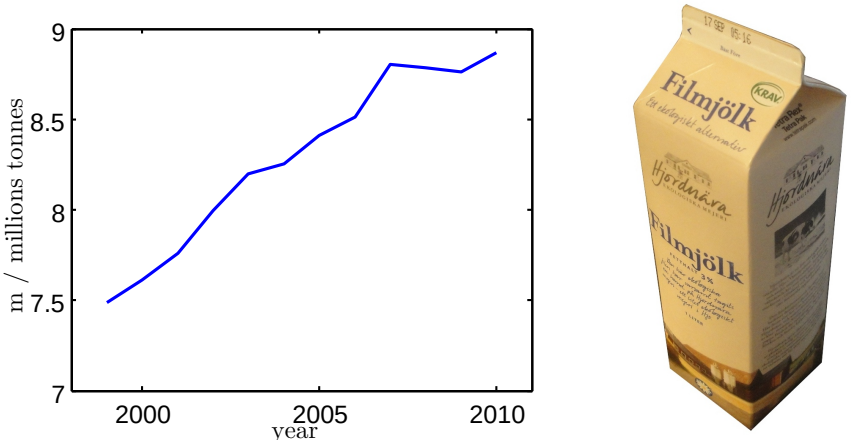

Figure 1.1: Left: obtained acidified milk for the 18 EU countries[2] for which Eurostat data was available from 1999 to 2010. [10] Right: filmjölk in a carton package.

most abundant proteins in milk are $\alpha_{s,1}$-casein and β-casein. The latter is a 224 amino acid unstructured protein, and is found both as monomers and in micelles. Upon decreasing the pH during the fermentation process, the properties of β-casein are dramatically changed when it dissociates from the colloids and is dissolved in the bulk. [1] Furthermore, caseins play a role in other surface adsorption phenomena like fouling at low pH. [8].

β-casein consists of a hydrophobic part near the C-terminal and a N-terminal positively charged head group, see Figure 1.2. A 25 amino acid group sequence in the head group has been shown to play an important role in precipitation, and is here referred to as bcn25. [9]

Fermented milk packages consist of up to six layers with a polyethylene coating on the outside to protect the package from getting wet, paperboard providing stiffness and strength, aluminium to protect from light and air, and plastic layers to seal the product. The innermost layer consists of polyethylene or polypropylene, which is usually oxidized. [11]

1.2 Aim

To design new, non-stick packaging materials a deeper understanding of the molecular basis of the adhesion of fermented milk on surfaces is essential.

Several mechanisms seem to be involved in the product loss of fermented milk. Firstly an initial layer adsorbs to the package material, and secondly a macroscopically large layer adheres to it.

Here, the physical chemical origin of the first effect is investigated, by simulating bovine β-casein near surfaces with different properties. A coarse grained model with implicit salt interactions needed to be developed and verified, and

[2]Belgium, Denmark, Germany, Estonia, Greece, Spain, France, Italy, Latvia, Lithuania, the Netherlands, Austria, Portugal, Slovenia, Slovakia, Finland, Sweden, and the United Kingdom

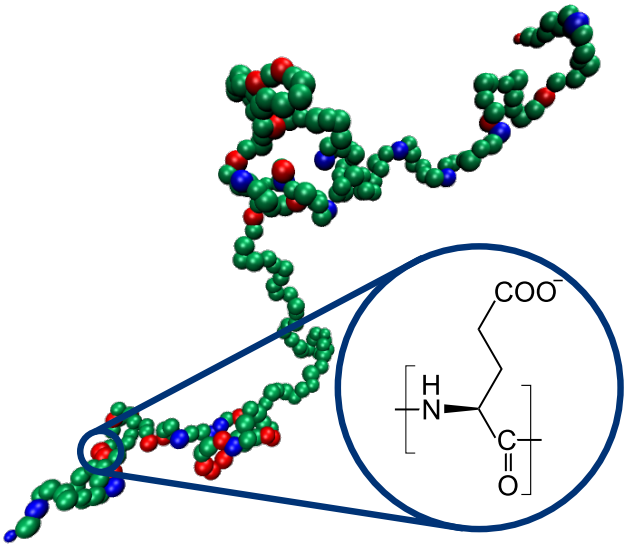

Figure 1.2: Amino acid representation of β-casein, where the red spheres are amino acid with negatively charged side chains, like the depicted glutamic acid, the blue spheres are positively charged, and the green spheres are neutral. The N-terminus is the blue sphere in the lower left.

the model is used to study both the mechanisms of β-casein adsorption, and adsorption as a function of different surface parameters.

Chapter 2

Polymer and polyelectrolyte theory

Polymers with charged groups are called polyelectrolytes. Unstructured proteins are special types of polyelectrolytes with amino acids as their repeating units. [12, 13] Casein in milk products is such an unstructured protein [13] and its basic properties can be described by the general theory for polymers [14, p. 358-362] and charged regulation. [15, 16]

Applied to the model developed in chapter 3, this theory will be referred to as the zero model, which is used to understand the complex interactions of β-casein with packaging material, as observed in chapter 5.

The two most easily accessible properties of a polymer in a solution are the end-to-end distance, R_{ee}, and the radius of gyration, R_g. This chapter discuss these properties as well as polymer repulsion from a hard wall, followed by simple models for the total charge, Z, and the charge capacitance, C, for polyelectrolytes.

2.1 End-to-end distance

The conformation of a polymer in solution can be described by a random walk model. In this model N_r monomers are regarded as point particles which are connected to their neighbours by bonds with a fixed bond length r_{eq}.

The end-to-end distance of the polymer R_{ee} then corresponds to the displacement length L_d of a random walk with $N_r - 1$ steps of length r_{eq}, see Figure 2.1. The root mean square (rms) displacement is described by diffusion theory

$$\left\langle R_{ee}^2 \right\rangle^{1/2} = \left\langle L_d^2 \right\rangle^{1/2} = (N_r - 1)^{1/2} r_{eq}. \tag{2.1}$$

The end-to-end distance increases thus linearly with the bond length, and increases with the square root of the number of monomers.

In this model the random walk may cross itself, while for a real polymer, the chain can not. The self-avoiding random walk may not cross itself and its end-to-end distance increases faster with the number of monomers

$$\left\langle R_{ee}^2 \right\rangle^{1/2} = (N_r - 1)^{\alpha} r_{eq} \tag{2.2}$$

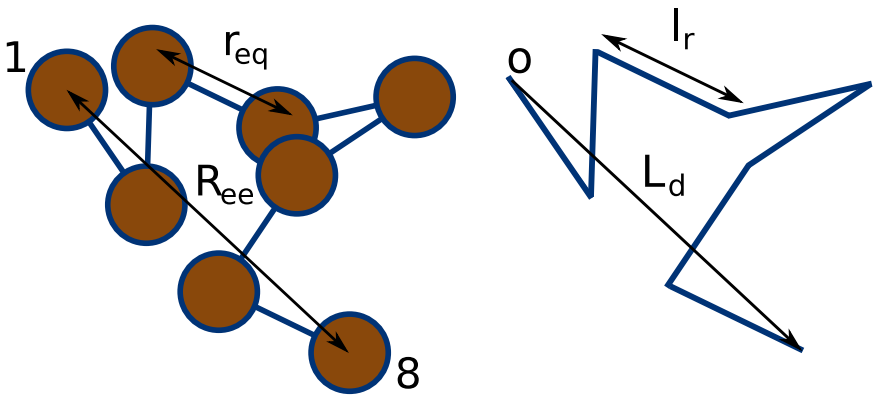

Figure 2.1: A polymer of 8 monomers bonded with bond length r_{eq} can be described by a random walk of 7 steps of length r_{eq} each, which total displacement, L_d, from the origin, o, corresponds to the polymer end-to-end distance, R_{ee}.

with $\alpha = 0.588$. [17]

For the random walk polymer in Figure 2.1, residues 4 and 6 overlap because of the small angle between monomers 4, 5, and 6. In a polymer the monomers cannot overlap and the bond angles can thus only have specific values, which results in a stiffness of the chain. This can be taken into account in the model by replacing the length between two monomers, r_{eq}, with a Kuhn length, $l_K > r_{eq}$, and the number of bonds with the number of Kuhn segments, N_k,

$$\left\langle R_{ee}^2 \right\rangle^{1/2} = N_k^{\alpha} l_K = \left(\frac{(N_r - 1) r_{eq}}{l_K} \right)^{\alpha} l_K = ((N_r - 1) r_{eq})^{\alpha} l_K^{1-\alpha} \tag{2.3}$$

$$\frac{\left\langle R_{ee}^2 \right\rangle^{1/2}}{r_{eq}} = (N_r - 1)^{\alpha} K_r^{1-\alpha}, \text{ with } K_r = \frac{l_K}{r_{eq}} \tag{2.4}$$

where we introduced the Kuhn ratio, K_r, which is the number of monomers per Kuhn segment.

If we estimate the Kuhn length to be twice the residue length, then for a 224 amino acid protein (like β-casein) with r_{eq} =4.9 Å (the typical distance between residues in a protein, as we will see later) and $\alpha = 0.6$, the end-to-end distance would be $(224 \cdot 4.9)^{0.6} \cdot 9.8^{0.4}$ Å = 166 Å.

Equation (2.4) is checked by simulating polymer chains with different numbers of monomers and monomer radii, and the resulting rms end-to-end distance is plotted in Figure 2.2.

If the monomer radius is negligible small, the polymer behaves as the simple random walk of (2.1) with $\alpha \approx 0.5$ and $K_r \approx 1$.

When the monomer radius increases, α increases to approximate the in literature found value for a self-avoiding random walk, because now the monomers will overlap if the chain crosses itself. The Kuhn length also increases, because the angular freedom is restricted due to monomer overlap.

For a polymer with 224 residues with r_{eq} = 4.9 Å and a monomer radius over residue length ratio of 0.65 (as in a peptide), an end-to-end distance of approximately 181 Å is obtained, in line with our earlier calculation. Note that in this model, electrostatic interactions and variations in the monomer radii are

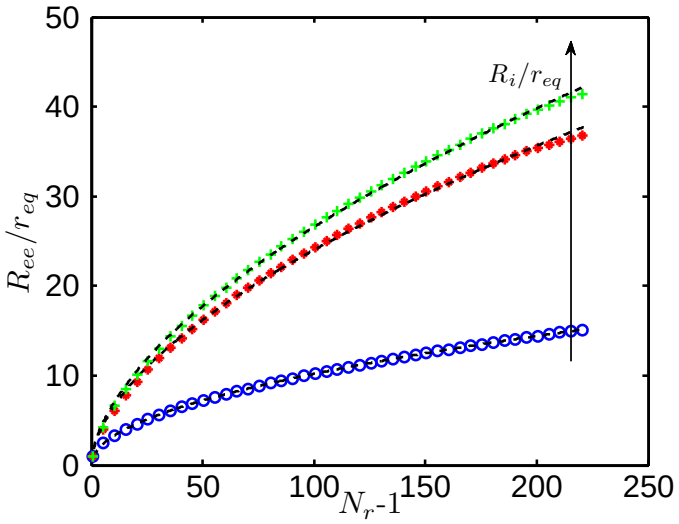

Figure 2.2: Rms end-to-end distance normalized with the bond length, R_{ee}/r_{eq}, as a function of the number of bonds, $N_r - 1$, for polymers with monomer radius over bond length ratios, $R_i/r_{eq} = 10^{-5}$ Å (o), 0.65 ($\star$) and 0.76 (+). The dotted lines are fits to (2.4) with coefficients $\alpha = 0.50, 0.57, 0.59$ and $K_r = 1.0, 3.5, 3.9$.

ignored.

2.2 Radius of gyration

Another quantity to describe the size of a polymer is the radius of gyration, R_g, which is the square root of the mass weighted sum over all monomers of the distances between each monomer $\mathbf{r}_i$ and the polymers centre of mass $\mathbf{r}_{cm}$

$$\left\langle R_g^2 \right\rangle^{1/2} = \sqrt{\frac{\langle \sum_{i=1}^{p} m_i |\mathbf{r}_i - \mathbf{r}_{cm}|^2 \rangle}{\sum_{i=1}^{p} m_i}} \tag{2.5}$$

with

$$\mathbf{r}_{\mathrm{cm}} = \frac{\sum_i m_i \mathbf{r_i}}{\sum_i m_i}. \tag{2.6}$$

This radius corresponds to the radius of homogeneous sphere which has the same diffusion properties as the polymer.

The ratio between the mean square end-to-end distance and radius of gyration gives an indication of the polymer conformation and is known as the shape factor

$$r_s = \frac{\left\langle R_{ee}^2 \right\rangle}{\left\langle R_g^2 \right\rangle}. \tag{2.7}$$

For a Gaussian coil, $r_s \approx 6$, while $r_s \approx 12$ if the polymer is totally stretched. If we solve (2.7) for R_g and substitute (2.4) for R_{ee}, a relation between the

polymer properties and the radius of gyration is obtained

$$R_g = \left\langle R_g^2 \right\rangle^{1/2} = \frac{\left\langle R_{ee}^2 \right\rangle^{1/2}}{\sqrt{r}} = \frac{r_{eq}(N_r - 1)^{\alpha} K_r^{1-.\alpha}}{\sqrt{6}} \tag{2.8}$$

where we assumed the coil to be ideal with $r_s = 6$

2.3 Interaction with a hard wall

Upon approaching a hard wall, a repulsive force acts on a polymer due to entropic effects. To model this force we consider the decrease in the number of configurations.

For a polymer consisting of non-interacting point monomers with a fixed intermonomer distance, the distribution of monomers in a polymer is obtained from simulations. The distribution is plotted in Figure 2.3a as a function of the relative z-distance from the centre of mass.

The obtained distribution corresponds to the distribution of all possible configurations over the monomer distances from the mass centre, and approaches a limiting distribution if $N_r \gg 1$. Fitting the normal distribution to the monomer distribution for $N_r = 224$ with $\sigma = .60R_g$, shows a similar shape for both distributions, but for the monomer distribution, the density is higher when $z_i = z_{\mathrm{cm}}$.

If the mass centre of the polymer approaches the wall, the number of configurations will decrease, because monomers can not move through the wall. We can assume that the number of configurations remains the same for $z_i - z_{cm} < z_{cm}$ and is zero otherwise.

This hypothesis is tested by simulating a point-particle polymer near a hard wall and plotting the distribution of the monomers as a function of both z_{cm} and $z_i - z_{cm}$ see Figure 2.3b. As expected the probability of finding a particle in the wall (at $z_i - z_{cm} > z_{cm}$) is zero, but the probability for $z_i - z_{cm} < z_{cm}$ also decreases with z_{cm}, resulting in a higher repulsion than expected.

A more extended theory derived by Eisenriegler and Maassen [18] accounts for these effects and gives an expression for the distribution of the centre of mass as a function of its distance from a hard wall,

$$g(z_{cm}) = \frac{3\sqrt{3}}{2\pi} \sum_{n=1,2,\ldots}^{\infty} B_n X_n e^{-X_n} \left[K_{1/3}(X_n) + K_{2/3}(X_n) \right] \tag{2.9}$$

with coefficients

$$B_n = \frac{1}{|a_n| \left[\mathrm{Ai}'(a_n) \right]^2} \left[\int_{a_n}^{\infty} \mathrm{Ai}(Y) dY \right]^2 \tag{2.10}$$

and z_{cm} contained in

$$X_n = \frac{2 |a_n|^3}{27 z_{cm}/R_g} \left[\int_{a_n}^{\infty} \mathrm{Ai}(Y) dY \right]^2 . \tag{2.11}$$

K_i are modified Bessel functions, a_n is the nth zero of the Airy function, Ai, and Ai$'$ is its derivative. This theory is checked for the distribution of our point

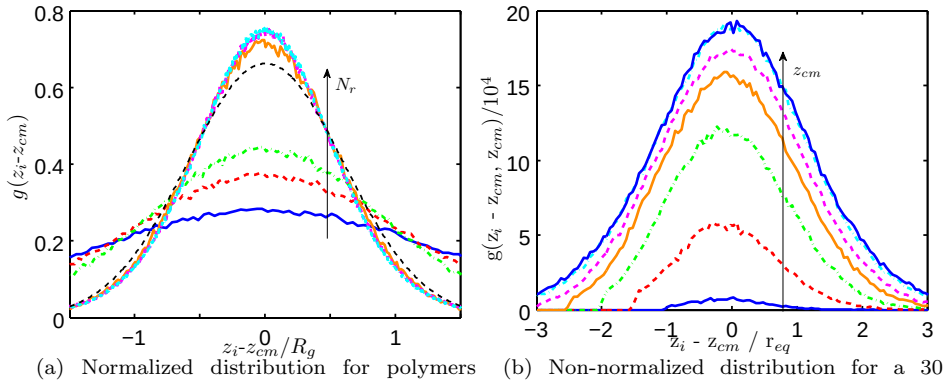

(a) Normalized distribution for polymers with number of monomers, N_r, 2 (—), 3 (– –), 4 (– ·), 10 (—), 100 (– –) and 224 (– ·), and a fit of the Gaussian distribution (3.27) to the $N_r = 224$ distribution (– –).

(b) Non-normalized distribution for a 30 monomer polymer, sampled for slices of $r_{eq}/10$ thickness at distances from a hard wall, z_{cm}/r_{eq}, 1.0 (—), 1.5 (– –), 2.0 (– ·), 2.5 (—), 3.0 (– –), 4.0 (– ·) and 5.0 (—).

Figure 2.3: Distributions of monomers as a function of the relative z-distance from the centre of mass.

polymers near a hard wall. When the degree of polymerization increases the distribution approaches the result of (2.9), see Figure 2.4 (left).

For a non-interacting polymer, the same result should be obtained from a bulk simulation if the distribution of the maximum displacement in the z-direction from the mass centre, $z_{\max}$, is sampled

$$g(z_{\max}) = f\left(\max_i(z_i - z_{cm})\right). \tag{2.12}$$

The coloured lines in Figure 2.4 (left) correspond to results from this approach. No significant difference is observed between the results from bulk simulations and wall simulations. In bulk it is easier to sample different configurations resulting in less statistical noise (or shorter simulations). Other interactions between the polymer and the wall as described in later chapters, can however not be taken into account by bulk simulations.

Finally we can obtain the free energy in $k_BT = \beta^{-1}$, the thermal energy, where k_B is the Boltzmann constant and T the temperature in K, from the mass centre distributions by applying

$$\beta\Delta A(z_{cm}) = -\ln g(z_{cm}) + \text{constant} \tag{2.13}$$

and the results are plotted in Figure 2.4b. The constant is chosen so that $z_{cm} \gg R_g$ corresponds to the standard state with $\Delta A = 0$. At $z_{cm} \approx 2R_g$ the free energy starts to increase and the polymer is repelled from the wall. For longer chain lengths, the free energy starts to increase at higher z_{cm}/R_g ratios, and the theoretical prediction is approached.

2.4 Total charge

The previous sections described general polymer properties. In addition to these properties, polyelectrolytes and unstructured proteins have a total net charge.

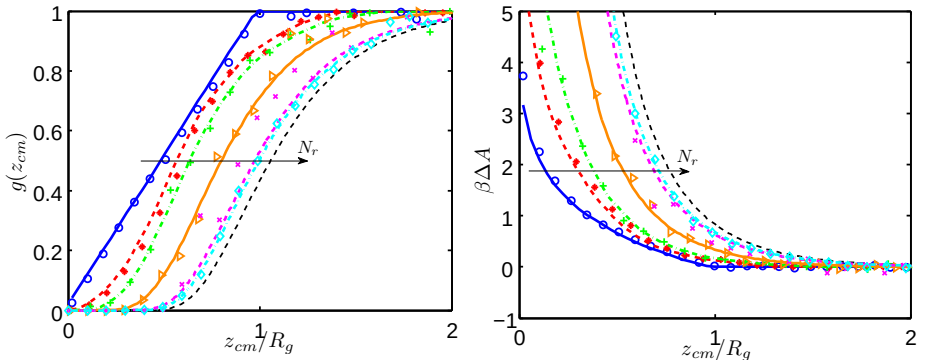

Figure 2.4: Polymer distribution, $g(z_{cm})$, as a function of the distance of its mass centre from a hard wall (left) and the corresponding free energy, $\beta\Delta A$, obtained from (2.13) (right) with number of monomers, N_r, 2 (o), 3 ($\star$), 4 (+), 10 ($\bullet$), 100 ($\times$) and 224 ($\diamond$). The black lines are obtained from (2.9) and the coloured lines from bulk simulations of $z_{\max}$.

The side chain of several amino acids and the C- and N-terminus of a peptide can be charged. The net sum of these charges can be estimated by following Lund and Jönsson [15] to obtain an expression for the total charge of a polyelectrolyte.

Acidic groups, RH, in a polyelectrolyte become negatively charged when a proton dissociates, leaving the conjugate base R^-

$$\mathrm{RH} \rightleftharpoons \mathrm{R}^- + \mathrm{H}^+ \tag{2.14}$$

while basic groups, RH^+, loose their charge when a proton dissociates

$$\mathrm{RH}^+ \rightleftharpoons \mathrm{R} + \mathrm{H}^+. \tag{2.15}$$

The reverse reaction, in which a proton reacts with a side chain, is called titration and RH and RH^+ are referred to as titrated groups.

Equations (2.14) and (2.15) can be generalized for any titration process of group $\mathrm{R}^{\,\mathrm{m}}$, with charge m$e$, by a titrant $\mathrm{X}^{\,\mathrm{n}}$, with charge n$e$, resulting in $\mathrm{RX}^{\,\mathrm{p}}$, with charge p$e$=(m+n)$e$, with e the elementary charge,

$$\mathrm{RX}^{\,\mathrm{p}} \rightleftharpoons \mathrm{R}^{\,\mathrm{m}} + \mathrm{X}^{\,\mathrm{n}}. \tag{2.16}$$

For the dissociation reaction of (2.16) a dissociation constant is defined from the concentrations, c_i, and the activity coefficients, γ_i,

$$K_d = \frac{c_{\mathrm{R}^{\,\mathrm{m}}} c_{\mathrm{X}^{\,\mathrm{n}}}}{c_{\mathrm{RX}^{\,\mathrm{p}}}} \frac{\gamma_{\mathrm{R}^{\,\mathrm{m}}} \gamma_{\mathrm{X}^{\,\mathrm{n}}}}{\gamma_{\mathrm{RX}^{\,\mathrm{p}}}} \approx \frac{c_{\mathrm{R}^{\,\mathrm{m}}} c_{\mathrm{X}^{\,\mathrm{n}}}}{c_{\mathrm{RX}^{\,\mathrm{p}}}} \tag{2.17}$$

where in the second step we assumed the activity coefficients to be unity. If $\mathrm{X}^{\,\mathrm{n}}$ is a proton, K_d is referred to as the acid dissociation constant, K_a.

Typical values of K_d span many orders of magnitude so

$$\mathrm{p}K_d = -\log_{10}(K_d) = -\log_{10}\left(\frac{c_{\mathrm{R}^{\,\mathrm{m}}} c_{\mathrm{X}^{\,\mathrm{n}}}}{c_{\mathrm{RX}^{\,\mathrm{p}}}}\right) \tag{2.18}$$

is usually tabulated in the literature. The pK_d values for the titratable amino acids and the C- and N-terminus are obtained from [19] and listed in appendix A.

The titrant concentration can also be expressed on a logarithmic scale

$$\mathrm{pX} = -\log_{10} c_{\mathrm{X}^{\mathrm{n}}} \tag{2.19}$$

which is the $\mathrm{pH} \equiv -\log_{10} \alpha_{\mathrm{H}^+} \approx -\log_{10} c_{\mathrm{H}^+}$ for proton titration.

Substituting this relation in (2.18) gives

$$\mathrm{p}K_d = \mathrm{pX} - \log_{10}\left(\frac{c_{\mathrm{R}^{\mathrm{m}}}}{c_{\mathrm{RX}^{\mathrm{p}}}}\right) \tag{2.20}$$

$$\frac{c_{\mathrm{R}^{\mathrm{m}}}}{c_{\mathrm{RX}^{\mathrm{p}}}} = 10^{\mathrm{pX}-\mathrm{p}K_d}. \tag{2.21}$$

This ratio is unitless so the concentrations can be replaced by the number of sites in moles, $n_{\mathrm{R}^{\mathrm{m}}}$ and $n_{\mathrm{RX}^{\mathrm{p}}}$,

$$\frac{n_{\mathrm{R}^{\mathrm{m}}}}{n_{\mathrm{RX}^{\mathrm{p}}}} = 10^{\mathrm{pX}-\mathrm{p}K_d}. \tag{2.22}$$

The mole fraction, x_i, is the number of i sites over the total number of sites, n_{tot}, and for R^{m}

$$x_{\mathrm{R}^{\mathrm{m}}} = \frac{n_{\mathrm{R}^{\mathrm{m}}}}{n_{\mathrm{RX}^{\mathrm{p}}} + n_{\mathrm{R}^{\mathrm{m}}}} = \frac{\frac{n_{\mathrm{R}^{\mathrm{m}}}}{n_{\mathrm{RX}^{\mathrm{p}}}}}{\frac{n_{\mathrm{RX}^{\mathrm{p}}} + n_{\mathrm{R}^{\mathrm{m}}}}{n_{\mathrm{RX}^{\mathrm{p}}}}} \tag{2.23}$$

$$= \frac{10^{\mathrm{pX}-\mathrm{p}K_d}}{1 + 10^{\mathrm{pX}-\mathrm{p}K_d}} \tag{2.24}$$

where in the last step (2.22) is substituted for $\frac{n_{\mathrm{R}^{\mathrm{m}}}}{n_{\mathrm{RX}^{\mathrm{p}}}}$.

Similarly, we can obtain an expression for the mole fraction of RX^{p}

$$x_{\mathrm{RX}^{\mathrm{p}}} = \frac{1}{1 + 10^{\mathrm{pX}-\mathrm{p}K_d}}. \tag{2.25}$$

In Figure 2.5 these expressions are used to plot the mole fractions as functions of the number of pX units away from the $\mathrm{p}K_d$. When $\mathrm{pX} = \mathrm{p}K_d$ ($\mathrm{pH} = \mathrm{p}K_a$ for proton titration) the exponents in (2.24) and (2.25) are zero and both mole fractions are $\frac{1}{2}$. At this particular pX the concentration of titrated and untitrated sites is thus equal.

If pX however decreases to lower values, the exponents are negative, resulting in a shift to more titrated sites, because the concentration X^{n} increases. For $\mathrm{pX} > \mathrm{p}K_d$ values, the titrant concentration is low and most sites are dissociated.

The average total charge for a peptide titrated by H^+ at a certain pH is the sum of the average charges per titratable site. This is simply the mole fraction of the charged form, either $-x_{\mathrm{R}^-}$ or x_{RH^+}. So, the total charge number of a peptide can be obtained by summing (2.25) over all basic groups b and subtracting the sum of (2.24) over the acidic groups a

$$\langle Z \rangle = \sum_b x_{\mathrm{RH}_{\mathrm{b}}^+} - \sum_a x_{\mathrm{R}_{\mathrm{a}}^-} \tag{2.26}$$

$$\langle Z \rangle = \sum_b \frac{1}{1 + 10^{\mathrm{pH}-\mathrm{p}K_{d,b}}} - \sum_a \frac{10^{\mathrm{pH}-\mathrm{p}K_{d,a}}}{1 + 10^{\mathrm{pH}-\mathrm{p}K_{d,a}}}. \tag{2.27}$$

This theory considers all titratable sites to be independent. The interactions between groups inside the peptide, and interactions with neighbouring water molecules and ions can be taking into account by computer simulations.

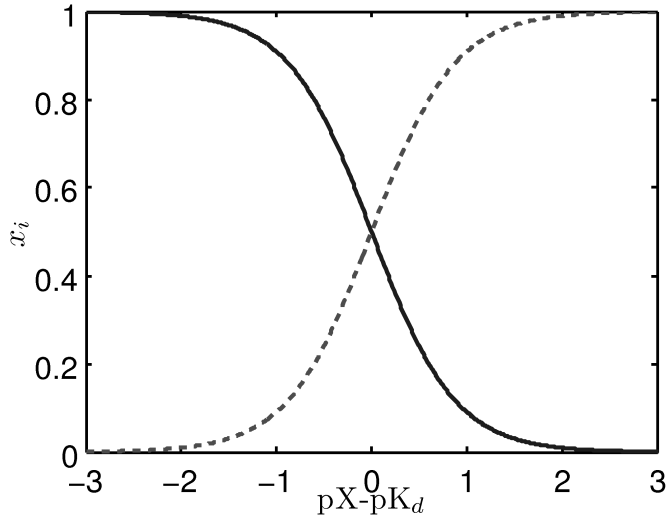

Figure 2.5: Mole fraction of titrated sites $x_{\mathrm{RX^P}}$ (**—**) and untitrated sites $x_{\mathrm{R^m}}$ (**– –**) as a function of the difference between the pX and pK_d.

2.5 Charge capacitance

The charge capacitance of a group, i, is defined as the change in mean charge number of the group, $\langle z_i \rangle$, upon a change in the electrostatic potential at the position of the group, $\Phi_{\mathrm{el}}(\mathbf{r}_i)$ [16]

$$c_i \equiv -\frac{1}{\beta e}\frac{\partial \langle z_i \rangle}{\partial \Phi_{\mathrm{el}}(\mathbf{r}_i)}. \tag{2.28}$$

To obtain a relation between the mean charge and the electrostatic potential we first consider the electrostatic interaction energy between a charge $z_i e$ and the potential

$$u_{\mathrm{el}}(\mathbf{r}_i) = z_i e \Phi_{\mathrm{el}}(\mathbf{r}_i). \tag{2.29}$$

The mean charge is now simply the thermodynamic average and for the NVT ensemble

$$\langle z_i \rangle = \frac{\sum z_i \exp(-\beta u_i)}{\sum \exp(-\beta u_i)} \tag{2.30}$$

$$= \frac{\sum z_i \exp(-\beta z_i e \Phi_{\mathrm{el}}(\mathbf{r}_i))}{\sum \exp(-\beta z_i e \Phi_{\mathrm{el}}(\mathbf{r}_i))} \tag{2.31}$$

where u_i is substituted with (2.29) in the second step and the sums are over all configurations.

Substituting this result in (2.28) yields

$$c_i = -\frac{1}{\beta e}\frac{\partial}{\partial \Phi_{\mathrm{el}}(\mathbf{r}_i)}\left[\frac{\sum z_i \exp(-\beta z_i e \Phi_{\mathrm{el}}(\mathbf{r}_i))}{\sum \exp(-\beta z_i e \Phi_{\mathrm{el}}(\mathbf{r}_i))}\right] \tag{2.32}$$

$$\begin{aligned} = -\frac{1}{\beta e}\Bigg[&\frac{\partial}{\partial \Phi_{\mathrm{el}}(\mathbf{r}_i)}\left[\sum z_i \exp(-\beta z_i e \Phi_{\mathrm{el}}(\mathbf{r}_i))\right]\frac{1}{\sum \exp(-\beta z_i e \Phi_{\mathrm{el}}(\mathbf{r}_i))} \\ &-\frac{\sum z_i \exp(-\beta z_i e \Phi_{\mathrm{el}}(\mathbf{r}_i))}{\left[\sum \exp(-\beta z_i e \Phi_{\mathrm{el}}(\mathbf{r}_i))\right]^2}\frac{\partial}{\partial \Phi_{\mathrm{el}}(\mathbf{r}_i)}\left[\sum \exp(-\beta z_i e \Phi_{\mathrm{el}}(\mathbf{r}_i))\right]\Bigg] \end{aligned} \tag{2.33}$$

$$\begin{aligned} = -\frac{1}{\beta e}\Bigg[&\left[\sum -\beta z_i^2 e \exp(-\beta z_i e \Phi_{\mathrm{el}}(\mathbf{r}_i))\right]\frac{1}{\sum \exp(-\beta z_i e \Phi_{\mathrm{el}}(\mathbf{r}_i))} \\ &-\frac{\sum z_i \exp(-\beta z_i e \Phi_{\mathrm{el}}(\mathbf{r}_i))}{\left[\sum \exp(-\beta z_i e \Phi_{\mathrm{el}}(\mathbf{r}_i))\right]^2}\left[\sum -\beta z_i e \exp(-\beta z_i e \Phi_{\mathrm{el}}(\mathbf{r}_i))\right]\Bigg] \end{aligned} \tag{2.34}$$

$$= -\frac{-\beta e}{\beta e}\left[\left\langle z_i^2\right\rangle - \left\langle z_i\right\rangle^2\right] = \left\langle z_i^2\right\rangle - \left\langle z_i\right\rangle^2. \tag{2.35}$$

The capacitance is thus simply the variance in the mean charge, e.g. the charge fluctuation.

To obtain a relation between the capacitance and the titration curve of a protein we have to relate the averages in (2.35) to pH, but first the energy difference between the associated RX^{p} and dissociated R^{m} state has to be obtained.

At equilibrium the states in a system are Boltzmann distributed and the concentration ratio between two states k and l with energies u_k and u_l is

$$\frac{c_k}{c_l} = \frac{e^{-\beta u_k}}{e^{-\beta u_;}}. \tag{2.36}$$

Substituting in the expression for the concentration ratio between the associated and dissociated state of (2.21) and rearranging, gives a relation between the titration energy u_{tit} and the pX

$$\frac{c_{\mathrm{RX}^{\mathrm{p}}}}{c_{\mathrm{R}^{\mathrm{m}}}} = e^{-\beta(u_{\mathrm{RX}^{\mathrm{p}}} - u_{\mathrm{R}^{\mathrm{m}}})} = e^{-\beta u_{\mathrm{tit}}} \tag{2.37}$$

$$10^{-(\mathrm{pX}-\mathrm{p}K_d)} = e^{-\beta u_{\mathrm{tit}}} \tag{2.38}$$

$$\beta u_{\mathrm{tit}} = (\mathrm{pX} - \mathrm{p}K_d)\ln 10. \tag{2.39}$$

If we define the energy of the untitrated state to zero, the energy of the titrated state is u_{tit} and the molecular partition function and charge averages for site i become

$$q = e^{-\beta u_k} + e^{-\beta u_l} = 1 + e^{-\beta u_{\mathrm{tit}}} \tag{2.40}$$

$$\left\langle z_i\right\rangle = \frac{m + p e^{-\beta u_{\mathrm{tit}}}}{q} \tag{2.41}$$

$$\left\langle z_i^2\right\rangle = \frac{m^2 + p^2 e^{-\beta u_{\mathrm{tit}}}}{q}. \tag{2.42}$$

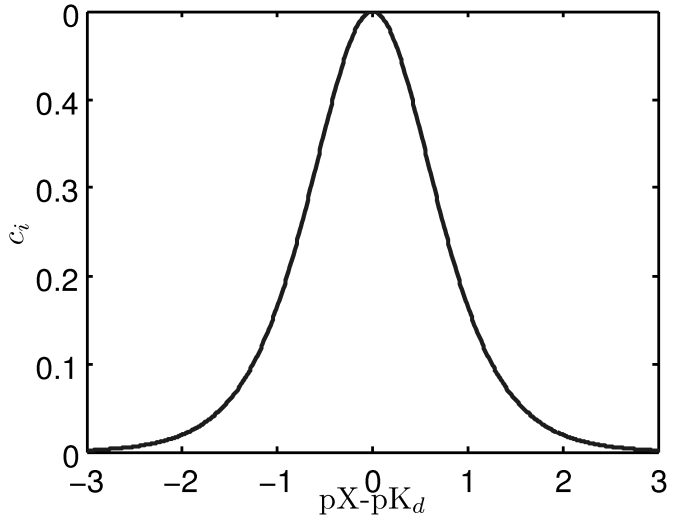

Figure 2.6: Charge capacitance as a function of the displacement of pX from the pK_d, calculated from (2.46) with $n = 1$.

Substituting these equations into (2.35) gives the capacitance as a function of pX and pK_d

$$c_i = \frac{m^2 + p^2 e^{-\beta u_{\text{tit}}}}{q} - \left(\frac{m + p e^{-\beta u_{\text{tit}}}}{q} \right)^2 \tag{2.43}$$

$$= \frac{m^2 + m^2 e^{-\beta u_{\text{tit}}} + p^2 e^{-\beta u_{\text{tit}}} + p^2 e^{-2\beta u_{\text{tit}}}}{q\left(1 + e^{-\beta u_{\text{tit}}}\right)} \tag{2.44}$$

$$- \frac{m^2 + 2mpe^{-\beta u_{\text{tit}}} + p^2 e^{-2\beta u_{\text{tit}}}}{q^2} \tag{2.45}$$

$$= \frac{n^2 e^{-\beta u_{\text{tit}}}}{q^2} = \frac{n^2}{4\left[\cosh\left(\frac{1}{2}[\text{pX} - \text{p}K_d]\ln 10\right)\right]^2} \tag{2.46}$$

where in the last step (2.39) is substituted in, and the hyperbolic cosine is recognized.

The charge capacitance depends thus only on the charge valency of the titrant and the displacement of pX from pK_d. Equation 2.46 is plotted in Figure 2.6. The hyperbolic cosine is symmetric around 0, where it has a minimum of 1. The capacitance is hence at a maximum for pX = pK_d with a value of $n^2/4$. If the pX displacement increases, the cosh becomes larger and eventually approaches infinity, giving a capacitance which approaches zero.

The change of the mean charge when pX is changed can be obtained by substituting (2.39) in (2.41) and taking the partial derivative with respect to

pX

$$\frac{\partial \langle z_i \rangle}{\partial \mathrm{pX}} = \frac{\partial}{\partial \mathrm{pX}} \left[\frac{m + pe^{-(\mathrm{pX}-\mathrm{p}K_d)\ln 10}}{q} \right] \tag{2.47}$$

$$= \frac{1}{q} \frac{\partial}{\partial \mathrm{pX}} \left[m + pe^{-(\mathrm{pX}-\mathrm{p}K_d)\ln 10} \right] + \left(m + pe^{-(\mathrm{pX}-\mathrm{p}K_d)\ln 10} \right) \frac{-1}{q^2} \frac{\partial}{\partial \mathrm{pX}} \left[1 + e^{-(\mathrm{pX}-\mathrm{p}K_d)\ln 10} \right] \tag{2.48}$$

$$= \frac{-\ln 10}{q} pe^{-(\mathrm{pX}-\mathrm{p}K_d)\ln 10} - \frac{-\ln 10}{q^2} \left(m + pe^{-(\mathrm{pX}-\mathrm{p}K_d)\ln 10} \right) e^{-(\mathrm{pX}-\mathrm{p}K_d)\ln 10} \tag{2.49}$$

$$= \frac{-\ln 10}{q^2} \left[pe^{-\beta u_{\mathrm{tit}}} \left(1 + e^{-\beta u_{\mathrm{tit}}} \right) - m \left(1 + e^{-\beta u_{\mathrm{tit}}} \right) e^{-\beta u_{\mathrm{tit}}} - ne^{-\beta u_{\mathrm{tit}}} e^{-\beta u_{\mathrm{tit}}} \right] \tag{2.50}$$

$$= \frac{-\ln 10}{q^2} ne^{-\beta u_{\mathrm{tit}}} = \frac{-\ln 10}{n} \frac{n^2 e^{-\beta u_{\mathrm{tit}}}}{q^2} \tag{2.51}$$

In the second part of the resulting equation, (2.46) is recognized, and finally a relation between the titration curve and the capacitance is obtained

$$c_i = -\frac{n}{\ln 10} \frac{\partial \langle z_i \rangle}{\partial \mathrm{pX}}. \tag{2.52}$$

The charge capacitance can thus be obtained from 1) the variance of the charge, 2) the shift of pX from the pK_d or 3) from the derivative of the titration curve with respect to the pX (pH for proton titration)

$$c_i \equiv -\frac{1}{\beta e} \frac{\partial \langle z_i \rangle}{\partial \Phi_{\mathrm{el}}(\mathbf{r}_i)} \tag{2.53}$$

$$= \langle z_i^2 \rangle - \langle z_i \rangle^2 \tag{2.54}$$

$$= \frac{n^2}{4 \left[\cosh \left(\frac{1}{2} [\mathrm{pX} - \mathrm{p}K_d] \ln 10 \right) \right]^2} \tag{2.55}$$

$$= -\frac{n}{\ln 10} \frac{\partial \langle z_i \rangle}{\partial \mathrm{pX}}. \tag{2.56}$$

Chapter 3

Model development

To simulate the behaviour of β-casein near packaging materials, a coarse grained model with implicit salt and water interactions is developed. The following estimation of the simulation time for a fully atomistic model makes it clear why such a model is necessary.

The properties of a protein depend on the other molecules it is interacting with. In a solution like milk, these other molecules are mainly water and salt particles, while fat particles and sugars are in the following discussion ignored.

In section 2.1 the end-to-end distance of a 224 amino acid peptide is estimated to be about 166 Å. If one simulates this peptide in a squared box with a side length of about twice the size of the end-to-end distance (to make sure the peptide does not interact with itself in a periodic box) the total volume of the box V is $(2 \cdot 166\text{Å})^3 = 4 \times 10^{-23}$ m^3. The number of water molecules in this box is

$$N_{\text{water}} = \frac{\rho N_A}{m} V \tag{3.1}$$

with ρ the density of water (1×10^3 kg/m^3), m its molecular mass (18.02 g/mol), and N_A Avogadro's constant (6.02×10^{23} mol^{-1}). Substituting in these number gives an approximate number of water molecules of 1×10^6, each consisting of three atoms.

For a 1:1 salt solution the number of ions in the box is

$$N_{\text{salt}} = (c_+ + c_-) V N_A \tag{3.2}$$

with c_+ and c_- the concentration cations and anions. For a salt concentration of 0.08 M (the ionic strength of milk [5, 6]) the resulting number of ions in our 4×10^{-23} m^3 simulation box is 2×10^3.

Finally the number of particles in a 224 amino acid peptide with approximately 20 atoms per residue is $224 \cdot 20 = 4 \times 10^3$.

About one million particles are thus present in the box, giving rise to $\binom{10^6}{2} = O(10^{11})$ pair interactions to be calculated after each Monte Carlo move. Pair interactions are distance dependent and the distance between particle i and j is to be calculated from Pythagoras' law

$$\mathbf{r}_{ij} = \sqrt{(x_i - x_j)^2 + (y_i - y_j)^2 + (z_i - z_j)^2} \tag{3.3}$$

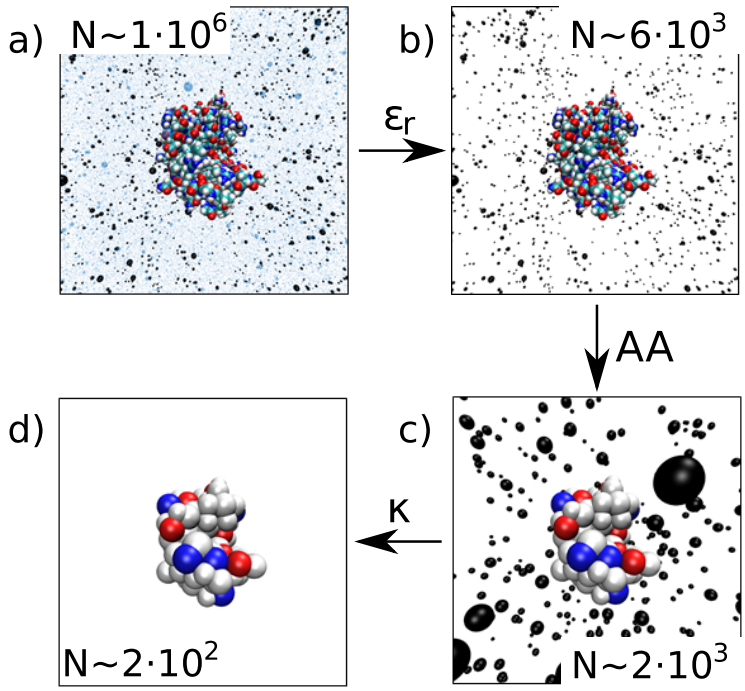

Figure 3.1: The number of interacting particles, N, is gradually decreased from about 1×10^6 to 2×10^2 by replacing explicit water particles by a dielectric constant ϵ_r; replacing the atoms in a peptide by coarse-grained particles representing one amino acid, AA, each and by taking into account the salt particles by a Debye screening length, κ^{-1}.

with x_n, y_n and z_n the position of particle n in three orthogonal directions.

In a computer simulation, the square root calculation is time-consuming, with about 80 cycles [20] per square root. Performing one million Monte Carlo steps on a GHz processor would thus take

$$t = 10^{11}\text{pairs} \times 10^6\text{steps} \times 10^2 \frac{\text{cycles}}{\text{pairs} \cdot \text{steps}} \cdot \frac{1}{10^9\text{Hz}} \tag{3.4}$$

$$= O(10^{10})\text{s} = O(10^2)\text{years} \tag{3.5}$$

Clearly we need to reduce the number of pair interactions to be able to perform our simulations on a more reasonable time scale. This is achieved by developing a model where the number of particles is decreased by introducing implicit interactions and coarse-graining the peptide, see Figure 3.1. The resulting number of interacting particles are the 224 amino acid residues and the simulation time thus becomes much more reasonable

$$t = \binom{224}{2}\text{pairs} \times 10^6\text{steps} \times 10^2 \frac{\text{cycles}}{\text{pairs} \cdot \text{steps}} \cdot \frac{1}{10^9\text{Hz}} \tag{3.6}$$

$$= O(10^4)\text{s} = O(10)\text{hours}. \tag{3.7}$$

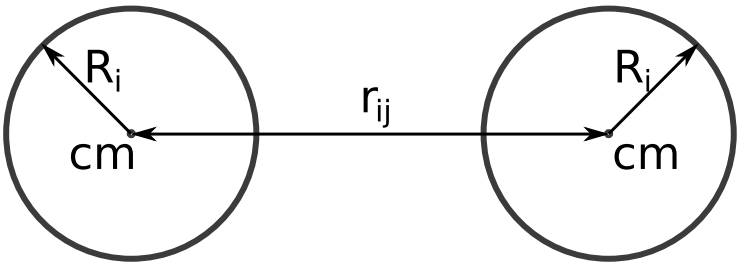

Figure 3.2: The pair interaction between two particles i and j depends on the distance between their centres of mass, $\mathbf{r}_{ij}$, and the radii R_i and R_j.

3.1 Non-bonded interactions

In the coarse-grained models of Figure 3.1c-d, we distinguish three different particle types: charged particles (salt particles and charged amino acids); hydrophobic amino acids and other amino acids. The model has three non-bonded interaction types: short-range Pauli repulsion, hydrophobic attraction and electrostatic interaction.

3.1.1 Pauli repulsion

At close contact particles repel each other due to overlapping electron orbitals. This effect is caused by the Pauli exclusion principle and is generally described by an $\mathbf{r}_{ij}^{-12}$ term

$$u_{\text{rep}}(\mathbf{r}_{ij}) = 4\epsilon \left(\frac{\sigma}{\mathbf{r}_{ij}} \right)^{12} \tag{3.8}$$

with ϵ a parameter for the interaction strength (typically .2 $k_B T$ [21]), σ the characteristic interaction distance, and $\mathbf{r}_{ij}$ the distance between the centres of mass of the particles i and j, see Figure 3.2.

In the coarse-grained model, each amino acid is represented by one particle with radius R_i and σ is the sum of the radii of two particles,

$$u_{\text{rep}}(\mathbf{r}_{ij}) = 4\epsilon \left(\frac{R_i + R_j}{\mathbf{r}_{ij}} \right)^{12}. \tag{3.9}$$

The amino acid radius can be estimated from the volume, V_i, of an amino acid, which is its molecular mass, m_i, over the density, ρ. The radius can then be obtained by assuming a spherical conformation

$$V_i = \frac{4}{3}\pi R_i^3 \tag{3.10}$$

$$R_i = \sqrt[3]{\frac{3}{4\pi}\frac{m_i}{\rho}} \tag{3.11}$$

where the volume is substituted with $\frac{m_i}{\rho}$ in the last step.

The protein density (1.41 g/dm^3) is taken as the limit for proteins with a molecular weight higher than 20 kDa (M_w = 25 KDa for β-casein), obtained

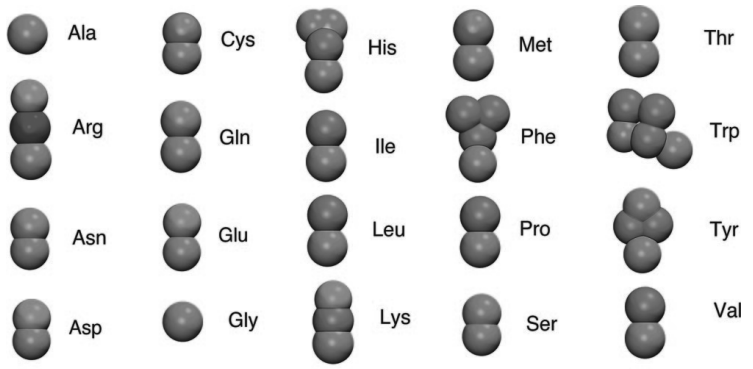

Figure 3.3: Representation of amino acid residues in the MARTINI force field. [21]

from an analysis of theoretical and experimental investigations by Fischer *et al.* [22].

The resulting radii are given in the `faunatoms.in` file, see appendix A with an average $\langle R_i \rangle = 3.2$ Å and $\langle R_i / r_{eq} \rangle = .65$. Using .9 g/dm^3 (the density of oil) as the average protein density would have given $\langle R_i \rangle = 3.7$ Å and $\langle R_i / r_{eq} \rangle = .76$.

The MARTINI coarse grained force field represents amino acids as a number of bonded spheres with a radius of 2.35 Å, see Figure 3.3. The average number of spheres per residue multiplied with the volume per sphere gives an average residue volume of 133 Å^3, which agrees well with $\langle V_i \rangle = 137$ Å^3 in our model.

The explicit salt model of Figure 3.1c also contains salt particles, with radii estimated to 2 Å as in [16].

3.1.2 Hydrophobic interactions

Hydrophobic interactions are caused by the attractive forces between apolar particles in water. Here, this interaction is modeled as an effective square potential

$$u_{\text{phob}}(\mathbf{r}_{ij}) = \begin{cases} -\epsilon_{\text{phob},ij} & \text{if } r_{ij} \leq r_{\text{phob}} \\ 0 & \text{if } r_{ij} > r_{\text{phob}} \end{cases} \tag{3.12}$$

where $\epsilon_{\text{phob},ij}$ is the hydrophobic interaction strength between particle i and j, and r_{phob} is the hydrophobic interaction distance. The interaction distance is estimated to be the size of a water molecule, 3 Å.

The interaction strength is residue dependent. The Eisenberg hydrophobicity scale [23] lists the hydrophobicity on a scale from very hydrophobic (.73) to not hydrophobic (-1.8).

In our simulations the seven residues with the highest values on this scale (ranging from .43 to .15 k_BT) are considered hydrophobic, while hydrophobic interactions are neglected for the others (ranging from .09 to -1.07 k_BT). If both particles are hydrophobic in this sense $\epsilon_{\text{phob},ij}$ is from chemical intuition set to .5 k_BT, while the interaction energy is zero otherwise. In `faunatoms.in` of appendix A the hydrophobicity of each amino acid residue is given.

3.1.3 Electrostatic interaction

In section 2.5 we saw for the electrostatic energy

$$u_{\text{el}}(\mathbf{r}_i) = z_i e \Phi_{\text{el}}(\mathbf{r}_i). \tag{3.13}$$

The electrostatic potential in this equation depends on the other charges in the system. In a gas phase the electrostatic potential at a distance $\mathbf{r}_j$ from a point charge j is

$$\Phi_{\text{el}}(\mathbf{r}_j) = \frac{z_j e}{4\pi\epsilon_0 r_j} \tag{3.14}$$

where ϵ_0 is the dielectric permittivity of a vacuum.

The interaction energy can now be obtained by substituting this equation in (3.13)

$$u_{\text{el}}(\mathbf{r}_{ij}) = \frac{z_i z_j e^2}{4\pi\epsilon_0 r_{ij}} \tag{3.15}$$

which is Coulomb's law.

In milk, charged particles are however not in a gas phase, but dissolved in water. As pointed out before, explicitly taking into account the effects of all individual water molecules on the interacting charges is too time-consuming. The solvent effect can however be approximated by replacing the water molecules by a dielectric continuum. Coulomb's law in such a continuum is

$$u_{\text{el}}(\mathbf{r}_{ij}) = \frac{z_i z_j e^2}{4\pi\epsilon_0\epsilon_r r_{ij}}. \tag{3.16}$$

The strength of the interaction energy is thus screened by a factor ϵ_r, which is the relative permittivity (80 in water).

By introducing the Bjerrum length,

$$\lambda_B = \frac{e^2}{4\pi\epsilon_0\epsilon_r k_B T} \tag{3.17}$$

(3.16) can be simplified and the total pair interaction energy in units of the thermal energy becomes

$$\beta u(\mathbf{r}_{ij}) = \beta u_{\text{el}}(\mathbf{r}_{ij}) + \beta u_{\text{rep}}(\mathbf{r}_{ij}) \tag{3.18}$$

$$= \frac{\lambda_B z_i z_j}{r_{ij}} + \beta 4\epsilon \left(\frac{R_i + R_j}{r_{ij}} \right)^{12} \tag{3.19}$$

where (3.8) is used to substitute for the repulsive part.

The obtained interaction energy consists of a long range r^{-1} attraction and a short range r^{-12} repulsion, and is used to obtain the interaction energy between charged particles in Figure 3.1c.

In the model of Figure 3.1d, however, the effect of salt particles is taken into account by an implicit interaction for which we use the Debye-Hückel theory. In this theory the potential around a spherical charged particle i with radius R_i is described as [14, p. 131-138]

$$\Phi_{\text{el}}(\mathbf{r}_i) = \frac{z_i e}{4\pi\epsilon_0\epsilon_r} \frac{\exp[-\kappa(r_i - R_i)]}{r_i(1 + \kappa R_i)} \tag{3.20}$$

in a salt solution with a Debye screening length,

$$\kappa^{-1} = \frac{1}{\sqrt{8\pi\lambda_B I N_A}} \tag{3.21}$$

with the ionic strength the sum over all ion species i, $I = \frac{1}{2}\sum_i c_i z_i^2$.

If $r_i \gg R_i$, Equation (3.20) becomes

$$\beta\Phi_{\text{el}}(\mathbf{r}_i) = \frac{\lambda_B z_i}{e}\frac{\exp[-\kappa r_i]}{r_i} \tag{3.22}$$

were we used (3.17) to substitute in the Bjerrum length. The electrostatic interaction energy is obtained by substituting this equation into (3.13)

$$\beta u_{\text{el}}(\mathbf{r}_{ij}) = \frac{\lambda_B z_i z_j}{r_{ij}} e^{-\kappa r_{ij}}. \tag{3.23}$$

The total pair interaction energy for charged particles is the sum of the electrostatic part and the repulsive part of (3.8)

$$\beta u_{\text{pair}}(\mathbf{r}_{ij}) = \frac{u_{\text{el}}(\mathbf{r}_{ij})}{k_B T} + \frac{u_{\text{rep}}(\mathbf{r}_{ij})}{k_B T} \tag{3.24}$$

$$= \frac{\lambda_B z_i z_j}{r_{ij}} e^{-\kappa r_{ij}} + \frac{4\epsilon}{k_B T}\left(\frac{R_i + R_j}{r_{ij}}\right)^{12}. \tag{3.25}$$

The effect of salt particles on the interaction energy is thus that the electrostatic part of (3.19) is screened with an exponential term, which decay length, κ^{-1}, is inversely proportional to the square root of the ionic strength. So at higher salt concentrations, the decay length is shorter and the screening is stronger.

Equation (3.25) is verified by comparing a simulation with explicit salt particles and particles interacting according to (3.19) (as in Figure 3.1c) with a simulation with implicit salt and particles interaction according to (3.23) (as in Figure 3.1d), see chapter 4 for more details about the simulation method.

The obtained pair potential between equally charged and oppositely charged particles are compared for both cases in Figure 3.4. Good agreement is observed between the explicit and implicit models.

3.2 Bonded interactions

The interaction between two neighbouring residues in a polypeptide chain is estimate from known crystal structures of bovine α-lactalbumin [24], β-lactoglobulin [25], lactoferrin [26], β-microglobulin [27] and soybean glycinin [28], which are obtained from the RCSB protein data bank.

Using these structures and (2.6), the mass centre of each amino acid residue, and the distances between each pair of neighbouring mass centres, $\mathbf{r}_{ij}$, can be calculated. A histogram of $\mathbf{r}_{ij}$ for each protein is presented in Figure 3.5 and the corresponding mean, μ, and standard deviation,

$$\sigma = \sqrt{\text{Variance}(x)} = \sqrt{\text{E}[(x-\mu)^2]} \tag{3.26}$$

are tabulated in Table 3.1.

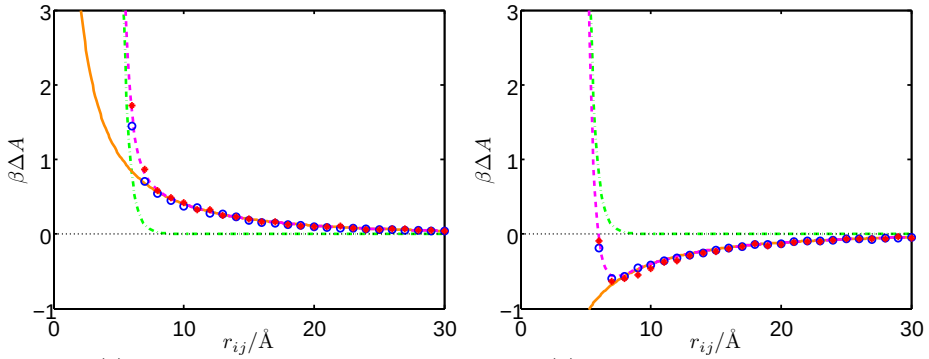

(a) Equally charged particles (b) Oppositely charged particles

Figure 3.4: Free energy, $\beta\Delta A$, as a function of the distance, r_{ij}, between two charged particles of radius 3 Å in a 30 mM 1:1 salt solution with explicit salt particles ($\star$) and implicit salt (o), and the Pauli repulsion (– ·) as calculated from (3.9), the electrostatic interaction (—) evaluated for each case (3.23), and the total interaction (– –) from (3.25).

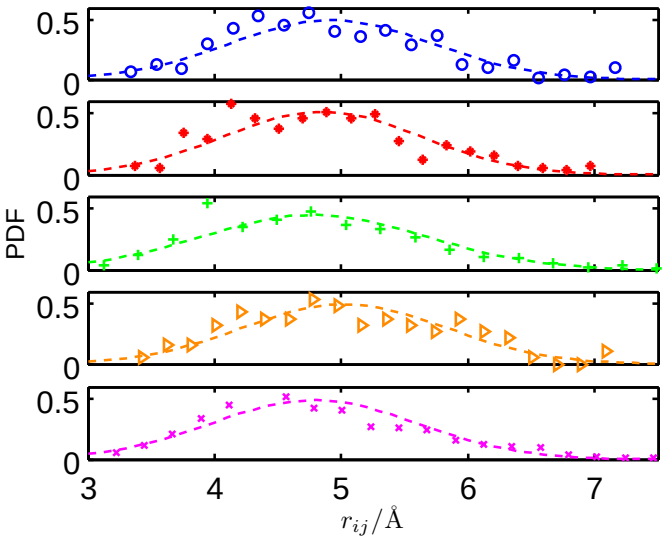

Figure 3.5: Probability distribution density of the distance between neighbouring amino acids, r_{ij}, in α-lactalbumin (o), β-lactoglobulin ($\star$), lactoferrin (+), β-microglobulin ($\bullet$) and glycinin ($\times$) and the distribution function calculated from the mean and standard deviation using (3.27) (lines).

Table 3.1: Mean, μ, and standard deviation, σ, of the distribution of amino acids distances in different proteins.

protein	μ/Å	σ/Å
α-lactalbumin	4.9	.80
β-lactoglobulin	4.9	.77
lactoferrin	4.8	.89
β-microglobulin	5.0	.80
glycinin	4.8	.81
average	4.9	.82

The probability density function for a Gaussian distribution of variable x with mean μ and standard deviation σ is [29, p. 1180]

$$\text{PDF(x)} = \frac{1}{\sigma\sqrt{2\pi}} \exp\left[-\frac{(x-\mu)^2}{2\sigma^2}\right]. \tag{3.27}$$

Using this equation the Gaussian PDF is plotted in Figure 3.5. As can be seen from the figure the distribution of $\mathbf{r}_{ij}$ in these proteins resembles indeed the form of a Gaussian distribution.

At equilibrium, the probability of finding a state i depends on its energy u_i

$$P(u_i) = \frac{\exp\left[-\beta u_i\right]}{\sum_i \exp\left[-\beta u_i\right]}. \tag{3.28}$$

Comparing (3.27) and (3.28) one can see that the relation between the energy and a Gaussian distributed variable should be

$$\beta u_i(x) = \frac{(x_i-\mu)^2}{2\sigma^2}. \tag{3.29}$$

So for the bond energy

$$\beta u_{\text{b}}(\mathbf{r}_{ij})) = \frac{1}{2\sigma^2}(r_{ij}-\mu)^2 \tag{3.30}$$

$$= k(r_{ij}-r_{eq})^2 \tag{3.31}$$

where we recognized the potential energy of a harmonic oscillator with equilibrium distance $r_{eq} = \mu$ and spring constant

$$k = \frac{1}{2\sigma^2}. \tag{3.32}$$

From Table 3.1 we obtain an equilibrium distance of about 4.9 Å for each protein; the standard deviation fluctuates more and has an average of .82, which corresponds to a spring constant of .76 Å^{-2}.

The equilibrium distance is thus smaller than twice the amino acid radius, which varies from 2.7 to 3.7 Å, see appendix A. This can be explained by the anisotropic shape of amino acids which side chains are perpendicular to the main chain. In the coarse grained model each residue is assumed to be spherical, making the spheres overlap.

3.3 External interactions

3.3.1 Charged surface

Interactions between charges on a surface and charged particles in a solution are described by the Gouy-Chapman theory [14, p. 131-138]. For a wall which is characterized by a surface charge density, σ in C/Å^2 or $\rho = \sigma/e$ in Å^{-2}, the Gouy-Chapman theory relates ρ and the electrostatic surface potential, Φ_0,

$$\rho = \frac{\sigma}{e} \tag{3.33}$$

$$= \sqrt{\frac{8k_BTI\epsilon_0\epsilon_r}{e^2}} \sinh\left(\tfrac{1}{2}\beta\Phi_0 e\right) \tag{3.34}$$

which is valid for a 1:1 salt solution with all symbols previously defined.

Solving (3.34) for the unit-less surface potential and recognizing the Bjerrum length (3.17) in the square root, one obtains the dimensionless surface potential

$$\beta\Phi_0 e = 2\sinh^{-1}\left(\rho\sqrt{\frac{\pi\lambda_B}{2I}}\right). \tag{3.35}$$

The dimensionless electrostatic potential at a distance z from the surface is given by

$$\beta\Phi_{\mathrm{el}}(z)e = 2\ln\left\{\frac{1+\Gamma_0\exp(-\kappa z)}{1-\Gamma_0\exp(-\kappa z)}\right\} \tag{3.36}$$

with κ^{-1} the Debye screening length (3.21), and Γ_0 the Gouy-Chapman parameter

$$\Gamma_0 = \tanh\left(\tfrac{1}{4}\beta\Phi_0 e\right) = \tanh\left(\frac{1}{2}\sinh^{-1}\left(\rho\sqrt{\frac{\pi\lambda_B}{2I}}\right)\right) \tag{3.37}$$

where (3.35) is substituted in.

The electrostatic pair interaction between a particle i with a charge z_i, at a distance z from a surface and the charges on the surface, can again be obtained by substituting the obtained expression for the potential into (3.13)

$$\beta u_{\mathrm{el,s}}(z) = z_i\beta\Phi_{\mathrm{el}}(z)e = 2z_i\ln\left\{\frac{1+\Gamma_0\exp-\kappa z}{1-\Gamma_0\exp-\kappa z}\right\}. \tag{3.38}$$

For a system with a given ionic strength and surface charge density we can thus calculate the Gouy-Chapman parameter using (3.37). The interaction energy between a charged particle and a surface at a distance z is then given by (3.38).

In our model this interaction is implemented as an external potential and the total energy for each particle is the sum of the pair interactions with all other particles and an external interaction dependent on its z-position.

For a single charged particle interacting with a charged surface this implicit model is compared to a model where a particle is interacting with explicit salt and surface point particles according to (3.16). From the distribution of charged

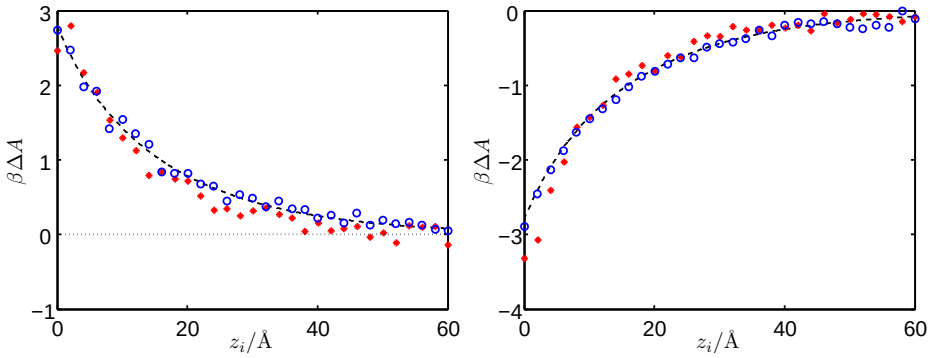

(a) Negatively charged particles

(b) Positively charged particles

Figure 3.6: The free energy, $\beta\Delta A$, as a function of the distance, z_I, from a negatively charged wall with 400 Å$^2/e$ and $I = 30$ mM for a system with implicit salt and surface particles (o) and a system with explicit salt and surface particles ($\star$); the dashed line is a plot of (3.38). In the explicit system the particles in solution have a radius of 2 Å, while the wall particles radius is 10^{-4} Å.

.

particles in both simulations, the free energy is obtained from (2.13) and plotted in Figure 3.6.

Good correlation is seen between the explicit and the implicit simulations, indicating that the Gouy-Chapman theory is indeed a valid approximation for interactions between small weakly charged particles in 1:1 salt and a surface with a low surface charge density.

If a titratable particle approaches a charged surface, its charge will be influenced by the surface potential. If we assume the charge to be Gaussian distributed with a standard deviation $\sigma = \sqrt{c_i}$, the charge at z is the mean bulk charge $\langle z_i \rangle$ minus a term which depends on the capacitance and the potential [16]

$$z_i(z) = \langle z_i \rangle - c_i \beta \Phi_{\text{el}}(z) e \tag{3.39}$$

and (3.38) becomes

$$\beta u_{\text{el,s}}(z) = \langle z_i \rangle \, \beta \Phi_{\text{el}}(z) e \; - \frac{c_i}{2} \left(\beta \Phi_{\text{el}}(z) e \right)^2 . \tag{3.40}$$

These equations are checked with simulations of the implicit model, see Figure 3.7. A good agreement between theory and simulation results is seen for small perturbations from the bulk charge, but when the mean particle charge approaches one, a deviation is observed, because the particle cannot take up more than one proton and the charge distribution deviates from a Gaussian distribution. This effect becomes more important in the low salt case, where a charge of up to 1.2 is predicted.

Comparing the free energy for the titratable particle, with the theoretical free energy if the capacitance is zero and the charge $z_i(z) = \langle z_i \rangle$, shows that the attraction becomes up to 50% stronger due to charge fluctuations.

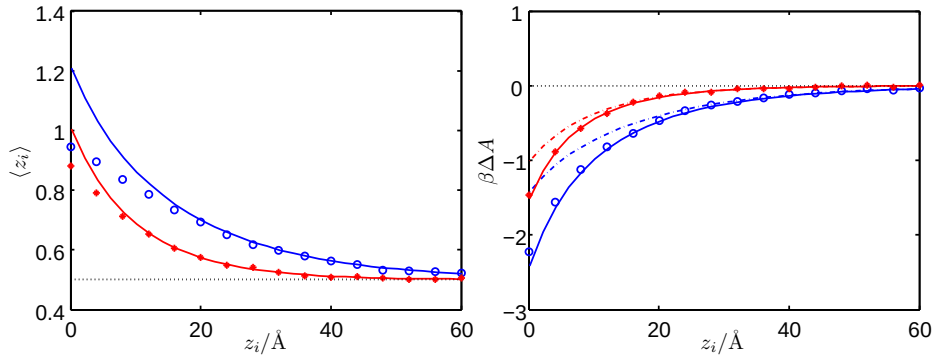

Figure 3.7: The mean charge, $\langle z_i \rangle$ (left), and free energy, $\beta\Delta A$ (right), of a titratable basic particle at pK_a=pH (and thus c_i=$\frac{1}{4}$, (2.46)) at distance z_i from a charged wall of $\rho = -.25$ nm^{-2} and in 30 mM (o) and 80 mM ($\star$) implicit salt. The solid lines are plots of (3.39) and (3.40), while the dashed-dotted line gives the free energy as calculated from (3.38) if the charge would have remained constant at $\langle z_i \rangle$.

Above equations are valid for point charges interacting with a potential at z, but a polyelectrolyte consists of many charges, each interacting with the potential at their position, $\Phi_{\rm el}(z_i)$.

The monomer distribution as a function of z_{cm} is discussed in section 2.3. If the polyelectrolyte charge and capacitance are assumed to be distributed in the same way, the electrostatic interaction can be integrated over the monomer positions with the monomer distribution $g(z_i, z_{cm})$ as a weight factor. The monomer distribution at z_{cm} is the bulk monomer distribution around 0, with the z-values shifted with z_{cm}.

For the net mean charge, (3.39) then becomes,

$$Z(z_{cm}) = \langle Z \rangle - \frac{\int_{z_i=0}^{\infty} C\beta\Phi_{\rm el}(z_i) e g(z_i, z_{cm}) dz_i}{\int_{z_i=0}^{\infty} g(z_i, z_{cm}) dz_i} \tag{3.41}$$

and for the free energy we obtain

$$\beta\Delta A(z_{cm}) = \frac{\int_{z_i=0}^{\infty} \left(\langle Z \rangle \beta\Phi_{\rm el}(z_i) e \ - \frac{1}{2} C \left(\beta\Phi_{\rm el}(z_i) e\right)^2 \right) g(z_i, z_{cm}) dz_i}{\int_{z_i=0}^{\infty} g(z_i, z_{cm}) dz_i}. \tag{3.42}$$

3.3.2 Hydrophobic surface

Hydrophobic interactions with a surface can be modelled as an external potential too. Now the potential energy is

$$u_{\rm phob,s}(z) = \begin{cases} -\epsilon_{{\rm phob},is} & \text{if } z \le r_{\rm phob} \\ 0 & \text{if } z > r_{\rm phob} \end{cases} \tag{3.43}$$

with $r_{\rm phob}$ again the hydrophobic interaction distance (3 Å) and $\epsilon_{{\rm phob},is}$ the hydrophobic interaction energy between particle i and the surface.

Chapter 4

Method

The described model in chapter 3 is used to investigate the system of interest. Fast estimations are made by sequence analysis in which properties per residue are calculated and averaged over a part or the whole protein. This method ignores interactions with other particles, and to include these, Monte Carlo simulations are also performed. Finally, an experimental titration curve of milk is obtained.

4.1 Metropolis Monte Carlo method

For a property B which depends on the coordinates, $\mathbf{r}$, of N particles, the thermodynamic average can be estimated by generating a set of random configurations, k, determining the energy in each state, U, and applying [30]

$$\langle B \rangle = \frac{\sum_k B(\mathbf{r}_k^N) \exp\left(-\beta U(\mathbf{r}_k^N)\right)}{Z} \tag{4.1}$$

with the partition function,

$$Z = \sum_k \exp\left(-\beta U(\mathbf{r}_k^N)\right). \tag{4.2}$$

The weight factor in these sums depends exponentially on the energy, so high energy states have a marginal contribution to the average.

In the Metropolis method [31, p. 23–31] a new configuration, l, is obtained by transforming an old configuration, k, and accepting the transformation with a probability

$$p_{\text{acc}}(k \to l) = \min\left\{1, \exp\left(-\beta \Delta U_{k \to l}\right)\right\} \tag{4.3}$$

where $\min\{a, b\}$ indicates the minimum of a and b. This method is also referred to as importance sampling, because here, in contrast to sampling random configurations, the states which contribute most to the macroscopic averages have the highest probability of being sampled.

The probability for a state to be sampled is thus

$$P(\mathbf{r}_k^N) = \frac{\exp\left(-\beta U(\mathbf{r}_k^N)\right)}{Z} \tag{4.4}$$

and thermodynamic averages can simply be calculated by averaging over the sampled configurations.

Finally, the Hemholtz free energy as a function of the particle position, $\Delta A(\mathbf{r})$, is simply related to the distributions of particle positions $g(\mathbf{r})$ by substituting $g(\mathbf{r})$ for $P({\mathbf{r_k}}^N)$ in (4.4), and solving for the energy difference between state $\mathbf{r}$ and a reference state

$$\beta\Delta A(\mathbf{r}) = -\ln(g(\mathbf{r})) + \text{constant}. \tag{4.5}$$

4.2 Monte Carlo simulations

Monte Carlo simulations were performed with the in house developed molecular simulation framework Faunus [32] which is open source and can be downloaded from `http://faunus.sourceforge.net`. The results presented in chapter 5 were obtained by simulations on Lunarcs cluster Platon running svn version 665 and 666 of the Faunus wall-protein programs. These programs were rewritten and extended for this research, and combine previously developed algorithms with newly designed functions.

A dedicated Matlab script was written to obtain amino acid sequences from the NCBI protein database `http://www.ncbi.nlm.nih.gov/protein` and to write out the corresponding `mol2` input file which defines the connectivity of the residues. Another script calculated the properties for each amino acid as defined in chapter 3 and writes these out to a `faunatoms.in` input file. Finally for each simulation a `wp.conf` file was written and an `eq.in` file which defines the titration pK_a values. Appendix A shows examples of these four input files.

The wallprotein programs read these four files to define a simulation box in the canonical ensemble (grand canonical if explicit salt was present) with the corresponding interaction parameters.

The protein was simulated in a cuboid simulation container with periodic boundary conditions, so that upon displacing a particle outside the box it entered from the other side, see Figure 4.1 (left). This periodicity reduces surface effects and was implied in all three dimensions for bulk simulations and in two dimensions for interactions with a wall.

Interactions were calculated using the minimum image convention in which a particle interacts with the nearest image of the other particles, as is illustrated with the dotted arrows in Figure 4.1 (left). The cuboid side length was chosen to be at least four times the rms end-to-end distance to prevent the polymer from interacting with its images as in the cartoon.

A Markov chain was started which randomly performed one of the following moves:

1. Randomly pick a monomer; translate each coordinate with a new random value between -.5·`monomer_dp` and .5·`monomer_dp`.

2. Translate each coordinate of the polymer as a whole with a random value between -.5·`moltrans_dp` and .5·`moltrans_dp`.

3. Rotate the polymer as a whole around a random axis with a random angle between -.5·`molrot_dp` and .5·`molrot_dp`.

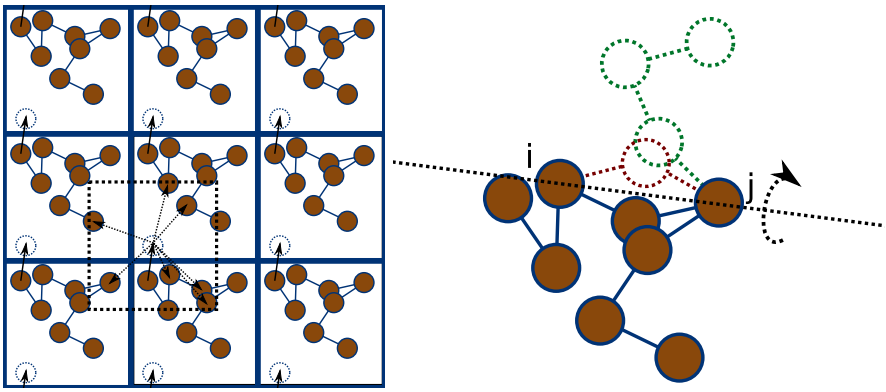

Figure 4.1: Left: 2D representation of a simulation box with periodic boundary conditions. Interactions are calculated with the minimum image convention, dotted lines. Right: crankshaft move (red dotted lines) and branchrot move (green dotted lines) around the axis between monomer i and j.

4. Randomly pick two monomers i and j; rotate all monomers between them around the axis r_{ij} with a random angle between -.5·`crankshaft_dp` and .5·`crankshaft_dp`, see Figure 4.1 (right).

5. Randomly pick two monomers i and j; rotate all monomers between the end closest to j and j itself around the axis r_{ij} with a random angle between -.5·`branchrot_dp` and .5·`branchrot_dp`, see Figure 4.1 (right).

6. Randomly pick a titratable monomer; swap for its counterpart.

and if salt particles or wall particles were present

7. Randomly pick a salt particle; translate each coordinate with a new random value between -.5·`saltmove_dp` and .5·`saltmove_dp`.

8. Randomly pick a wall particle; translate the x and y coordinate with a random value between -.5·`wall_dp` and .5·`wall_dp`.

9. Insert a Na^+ Cl^- pair at a random position or remove a random Na^+ Cl^- pair.

The values of the displacement parameters `moves_dp` were read from `wp.conf` and optimized by running a simulation of a representative system in which the displacement parameters where randomly chosen between two cutoffs. The displacement parameter which resulted in a) the largest rms displacement of the position (for moves 1, 2, 7 and 8) or b) the largest change in the radius of gyration (for moves 4 and 5) was used in the other simulations.

After each move the energy difference between the original and transformed state was determined by summing over the interactions of all transformed particles i with all particles in the system N

$$\Delta U = \sum_{i}^{\text{moved}} u(\mathbf{r}_{i,\text{new}}, \mathbf{r}^N_{\text{new}}) - \sum_{i}^{\text{moved}} u(\mathbf{r}_{i,\text{old}}, \mathbf{r}^N_{\text{old}}) \tag{4.6}$$

and the new state was accepted with the probability of (4.3).

The energy terms in (4.6) are

$$u_i(\mathbf{r}_i, \mathbf{r}^N) = \left[\sum_{j \neq i}^{\mathrm{N}} u_{\mathrm{pair}}(\mathbf{r}_{ij}) + \sum_{j \neq i}^{\mathrm{bonded}} U_{\mathrm{b}}(\mathbf{r}_{ij}) + u_{\mathrm{el,s}}(z_i) + u_{\mathrm{phob,s}}(z_i) + u_{\mathrm{tit}} \right]. \tag{4.7}$$

The pair interaction energy was calculated using a new tabulation algorithm

$$\beta u_{\mathrm{pair}}(\mathbf{r}_{ij}) = \begin{cases} \frac{\lambda_B z_i z_j}{r_{ij}} e^{-\kappa r_{ij}} + u_{\mathrm{rep}}(\mathbf{r}_{ij}) + u_{\mathrm{phob}}(\mathbf{r}_{ij}) & \text{if } r_{ij}^2 > r_{\mathrm{max}}^2 \\ \left\{ z_i z_j \beta \left[\Phi_{\mathrm{el}} \left(\mathrm{res} \left\lfloor \frac{r_{ij}^2}{\mathrm{res}} \right\rfloor \right) + \right. \right. & \\ \left. \left. \frac{\Phi_{\mathrm{el}} \left(\mathrm{res} \left\lceil \frac{r_{ij}^2}{\mathrm{res}} \right\rceil \right) - \Phi_{\mathrm{el}} \left(\mathrm{res} \left\lfloor \frac{r_{ij}^2}{\mathrm{res}} \right\rfloor \right)}{r_{\mathrm{res}}^2 \left\lceil \frac{r_{ij}^2}{r_{\mathrm{res}}^2} \right\rceil - r_{\mathrm{res}}^2 \left\lfloor \frac{r_{ij}^2}{r_{\mathrm{res}}^2} \right\rfloor} \right] + u_{\mathrm{rep}}(\mathbf{r}_{ij}) + u_{\mathrm{phob}}(\mathbf{r}_{ij}) & \text{if } r_{\mathrm{max}}^2 > r_{ij}^2 > r_{\mathrm{min}}^2 \\ 0 & \text{if } r_{ij}^2 < r_{\mathrm{min}}^2 \end{cases} \tag{4.8}$$

$\Phi_{\mathrm{el}}(r_{ij}^2)$ was a tabulated version of (3.22) for r_{ij}^2 with a resolution res in Å^2 (`tabpot_r2`) and ranging from r_{min}^2 (corresponding to an electrostatic energy of `tabpot_Umax`) to r_{max}^2 (corresponding to `tabpot_Umin`). Values were extracted from the table for the upper limit using `ceil` operators, $\lceil\rceil$, and the lower limit using `floor` operators, $\lfloor\rfloor$.

This algorithm avoids the expensive square root calculation at large interaction distances, while giving an exact result at close contact. For a typical simulation with `tabpot_Umin`=.1, `tabpot_Umax`=10^{-6} and `tabpot_dr2`=1 this results in a twice as fast simulation speed and a maximum error in the energy of $1.4 \times 10^{-5} k_B T$ at r_{ij}=5.8 Å.

The repulsive and hydrophobic terms were defined by (3.9) and (3.12). The second term in (4.7) was the sum of the bond energy (3.31) over all particles bonded to i. The third term was only non-zero for charged particles in the presence of a Gouy-Chapman wall and the energy was calculated by interpolating a tabulated version of (3.36) and multiplying with the particle charge. The last terms were only non-zero for hydrophobic particles interacting with a hydrophobic wall with energy (3.43), and for the titration move with u_{tit} as defined in (2.39).

If the polymer was confined, moves were always rejected if the centre of mass was displaced outside the slice. Individual monomers were however free to move outside the slice.

For salt insertion and extraction, the energy difference consisted of a contribution from the inserted and removed particles, and a contribution which

depended on the bulk chemical potential μ_i^b (`MUs`)

$$\Delta U_{\text{ins}} = \sum_i^{\text{ins}} \left[\sum_{j \neq i}^{\text{all}} u_{\text{pair}}(\mathbf{r}_{ij}) - \mu_i^b + k_B T \ln \frac{N_i}{V} \right] \tag{4.9}$$

$$\Delta U_{\text{rem}} = - \sum_i^{\text{ins}} \left[\sum_{j \neq i}^{\text{all}} u_{\text{pair}}(\mathbf{r}_{ij}) - \mu_i^b + k_B T \ln \frac{N_i}{V} \right] \tag{4.10}$$

where N_i was the total number of ion i particles in the simulation container with volume V.

The monomer move, titration, salt move and wall particle move steps are repeated for the number of monomers, titratable sites, salt particles and wall particles respectively, while all other steps are performed ones per microstep.

The loop was (`macrosteps`+1)×`microsteps` times performed, where `macrosteps` was 10, and `microsteps` 10^6 for protein-wall simulations, 10^5 for bulk simulations and 10^4 for simulations in explicit salt. The system equilibrated during the first `microsteps` moves, while properties are sampled during the rest of the simulation, with a probability of .3 after each microstep.

After each macrostep the energy in the system was calculated by summing over all particle interactions. This value was compared to the sum of all ΔU plus the begin energy and the difference was defined as the energy drift, which should be about zero.

$$\sum_{\text{steps}} \Delta U + U_{\text{init}} - U_{\text{final}} \approx 0. \tag{4.11}$$

4.3 Acid titration

To a milk sample (Skånemejerier mellanmjölk, 3 g fat, 3.5 g protein) hydrochloric acid was added, and from the measured pH as a function of the added volume a capacitance curve was obtained.

As a titrant, 0.1 M hydrochloric acid was added five drops at a time with a burette, and the pH was measured under stirring with a Eutech Instruments pH meter with a glass electrode. The charge of the titrated particles was proportional to the difference between the number of protons added and the number of free protons in the solution

$$Q \propto n_{\text{H}^+,\text{added}} - n_{\text{H}^+,\text{free}} \tag{4.12}$$

$$\propto V_{\text{titrant}} c_{\text{H}^+,\text{titrant}} - [V_{\text{titrant}} + V_{\text{analyte}}]\, c_{\text{H}^+} \tag{4.13}$$

$$\propto V_{\text{titrant}} c_{\text{H}^+,\text{titrant}} - [V_{\text{titrant}} + V_{\text{analyte}}]\, 10^{-\text{pH}} \tag{4.14}$$

and the derivative with respect to pH gave the capacitance in arbitrary units.

Chapter 5

Results

In this chapter, simulations results for casein in bulk and near packaging materials are presented, and discussed with the assembled zero model.

In the first section, the bulk behaviour of β-casein and bcn25 is described. Bcn25 is identified as an active part of β-casein in surface interactions, and here it is used to compare results for the implicit and explicit salt model. Furthermore, the presented ideas from chapters 2 and 3 are firstly used to understand the simulation results for bcn25, before applying them on the more complex behaviour of β-casein.

Having verified the model, and identified the characteristic properties of β-casein in the first section, the second section present simulation results for the adsorption on package material. Again, bcn25 is used as a model peptide to compare with explicit salt simulations and to introduce the main principles, but the main part of this section contains a discussion of the adsorption mechanism for β-casein on different surfaces, and the influence of surface and solution properties on the interaction.

5.1 Bulk behaviour

5.1.1 Total charge

For the sequence of bcn25[1], the mean charge per residue is calculated from (2.27) with the pK_a values from appendix A at pH 6.7 (measured for normal milk) and 4.5 (measured for fermented filmjölk).

In Figure 5.1a this zero model, which does not take into account interactions between charged particles, is compared with simulations of the peptide in implicit and explicit salt. Furthermore the position of the hydrophobic sites is given.

Hydrophobic interactions are not taken into account in the explicit salt simulations and in order to compare explicit and implicit salt simulations, hydrophobic interactions are ignored for bcn25.

At pH 6.7, all residues are either fully protonated or deprotonated and the same result is obtained with the three methods. When pH decreases to 4.5, however, the glutamic acid (E) pK_a of 4.1 is approached and the negative mean

[1] releelnvpgeiveslssseesitr [9]

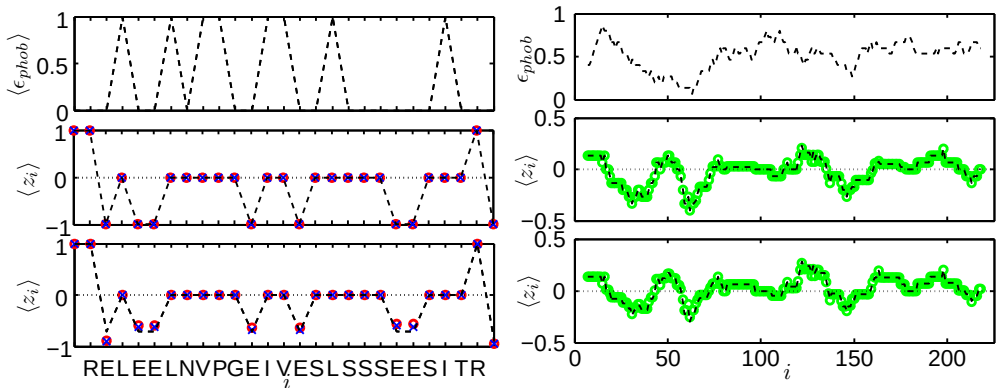

(a) bcn25 (b) β-casein

Figure 5.1: Hydrophobicity per residue, ϵ_{phob}, (top) and mean charge per residue, $\langle z_i \rangle$, at pH 6.7 (middle) and 4.5 (bottom). For β-casein the 15-residue moving averages are given. The zero model values for the charge are calculated from (2.27) (– –). For bcn25 simulation results are presented for 30 mM explicit ($\times$) and implicit salt (o), and for β-casein simulation results at 80 mM implicit salt (o) are shown.

charge of the glutamic acid residues is partly neutralized. At this pH, the predictions from (2.27) are only exact for the single sites, while in both the implicit and explicit salt simulations two neighbouring glutamic acid sites have slightly less negative charge and the glutamic acid residue close to two positively charged sites has more negative charge.

The 224 amino acid sequence of bovine β-casein[2] results in a much larger peptide than bcn25, and while for bcn25 a 375^3 Å^3 simulation box was sufficiently large as is shown later, β-casein needs a box of 1000^3 Å^3, which has a 19 times larger volume and hence about $19^2 = 361$ as many pair interactions. This makes explicit salt simulations too time-consuming for β-casein. Therefore, only implicit simulations and the zero model are compared in Figure 5.1b, which shows the 15 amino acid moving average of the mean residue charge. By averaging over 15 residues, the small errors for partly charged sites cancel and a perfect agreement is seen.

At pH 6.7 the first 70 residues of β-casein contain two negatively charged regions, while the remaining residues are net neutral. The glutamic acids in the bcn25 part of β-casein correspond to the first minimum in the mean charge. The moving averages indicate that the latter part is also more hydrophobic, while the negatively charged regions are not. This amphiphilic character lessens when pH is decreased and the protein contains alternating positively and negatively charged regions.

The sum of each residual mean charge gives the mean net charge which as a function of pH is a so-called titration curve, see Figure 5.2. The total charge decreases from $+3e$ at pH=1 to $-8e$ at pH=14 for bcn25 and from $+23e$ to $-29e$

[2] mkvlilaclvalalareleelnvpgeiveslssseesitrinkkiekfqseeqqqtedelqdkihpfaqtqslvyp fpgpihnslpqnippltqtpvvvppflqpevmgvskvkeamapkhkempfpkypvepftesqsltltdvenlhlplpllq swmhqphqplpptvmfppqsvlslsqskvlpvpqkavpypqrdmpiqafllyqepvlgpvrgpfpiiv [33]

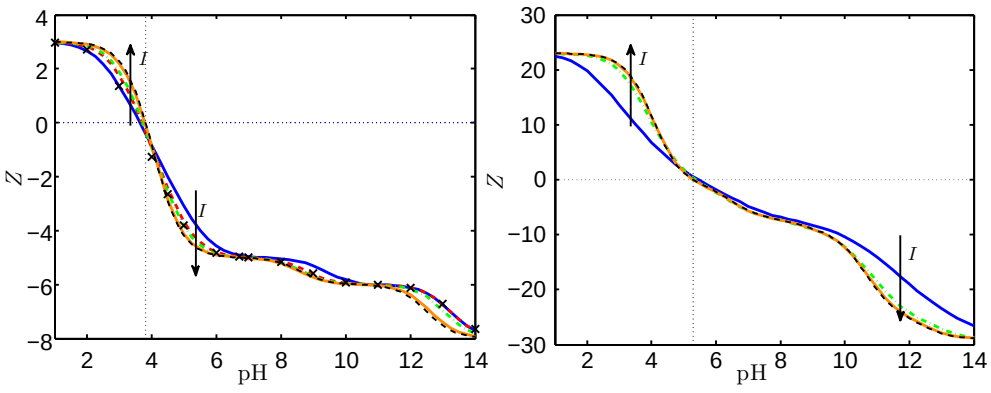

(a) bcn25 (b) β-casein

Figure 5.2: The total mean charge as a function of pH as calculated from (2.27) (– –) and from computer simulations with implicit salt of I/mM 0 (—), 30 (– –), 80 (– ·) and 10^3 (—) and explicit 30 mM salt (×). The vertical dotted lines indicates the zero model isoelectric point.

for β-casein. At pH $\approx$ 5.5, β-casein has no net charge and this pH value is referred to as the isoelectric point, pI.

For bcn25, pI $\approx$ 4, close to the pH of fermented milk, whereas for normal milk (pH $\approx$ 6.7) bcn25 is highly charged, with a net charge of about -5e for only 25 amino acids, corresponding to the 8 negatively and 3 positively charged residues in Figure 5.1a.

At 1 M ionic strength, the Debye length approaches zero and electrostatic interactions are almost completely screened, giving a very good agreement between theory and experiment.

When the peptides are titrated at low ionic strength electrostatic interactions are unscreened and it will be more costly to take up another charge for an already net charged protein. This results in a lower net charge if pH<pI and a higher net charge if pH>pI, making the titration curves cross at the isoelectric point.

Implicit and explicit salt simulations for bcn25 show good agreement.

5.1.2 Charge fluctuations

The net charge of a peptide fluctuates around the mean charge and its distribution for β-casein at 80 mM and at different pH values is presented in Figure 5.3.

At pH 1, all charged sites are titrated and the net charge is stable at +23. Increasing pH to 3-5, the net charge decreases steeply and large fluctuations are seen, since many acidic sites have their pK_a values around 4. At pH 7-9, the net charge changes slightly with pH and does not fluctuate much, because of the low number of titratable sites with pK_a values around 8 in the protein. Upon increasing pH even more, large fluctuations and a steep charge decrease are observed at the pK_a of the basic groups and finally the charge stabilizes at pH 14.

Protein charge fluctuations thus increases when pH is near the pK_a of its residues and the net charges changes a lot, in perfect agreement with the rela-

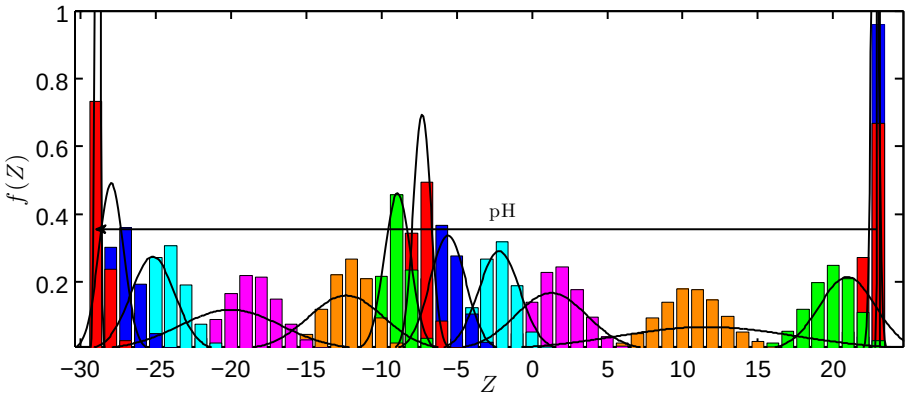

Figure 5.3: Probability density distribution of the β-casein net charge, Z, for simulations with 80 mM implicit salt at pH from 1 (blue) to 14 (red) with steps of pH 1, and the Gaussian distribution calculated for each pH by using the zero model charge fluctuation (2.46) and mean charge (2.27) in (3.27) (—).

tions derived in section 2.5.

In section 3.3.1, the net charge distribution is assumed Gaussian and a plot of the normal distribution around the mean charge from the zero model with a variance of the zero model capacitance (2.46) is compared with the simulation results in Figure 5.3

At most pH values good agreement is seen between the zero model and simulation results, but when pH is near the pK_a value of many residues, electrostatic interactions play a more important role and the zero model does not predict the exact behaviour.

In Figure 5.4, a high capacitance is observed for β-casein around pH 4 and 10, as in Figure 5.3, while the capacitance approaches zero at both pH extremes. Bcn25 has an additional maximum at pH 9 and the first maximum occurs at pH $\approx$ pI $\approx$ 4, the region where the glutamic acid residues are partly charged, as already seen in Figure 5.1.

At high ionic strength good agreement is seen between zero model and simulations. Upon decreasing the ionic strength, however, it becomes increasingly more costly to take up additional charges, when the peptide has been charged up, and the curves right shift for pH $>$ pI and left shift for pH $<$ pI. Only the position of the curve at pH = pI remains the same.

From the relation between the capacitance and the derivative of the titration curve, it is understood that the area under the curve remains the same, which leads to broader peaks in the low salt case. The explicit salt simulations for bcn25 at 30 mM show again a perfect agreement with implicit salt simulations.

Finally, these results are compared with the experimentally obtained derivative of the titration curve of normal milk, which is linear with the capacitance (2.52). At pH$<$3 a large peak is observed, which is probably due to oxidation reactions and not to proton titration. The peak at the isoelectric point probably corresponds to the peak at pH 4 in the simulations, while pH for the shoulder at 6-7, coincides with the peak at this pH in the simulation results.

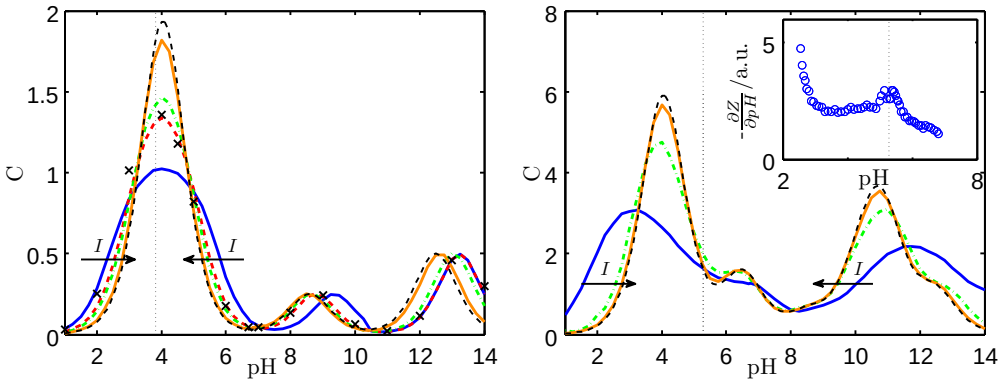

(a) bcn25 (b) β-casein

Figure 5.4: Capacitance C as a function of pH as calculated from (2.46) (– –) and from the charge variance in computer simulations with 30 mM explicit salt ($\times$) and implicit salt of I/mM 0 (—), 30 (– –), 80 (– ·) and 10^3 (—). The inset gives the experimental result for normal milk.

Upon adding concentrated hydrochloric acid to milk, it has been observed by visual inspection, that the viscosity of the liquid increases and a yoghurt like substance is obtained. The precise capacitance dependence on the pH for β-casein, however, can not be obtained from titration curves on the complex milk sample.

5.1.3 Shape

The influence of pH and ionic strength on the shape of both bcn25 and β-casein is investigated through R_g, R_{ee} and r_s, see Figure 5.5.

At high ionic strength electrostatic interactions are screened and R_{ee}, R_g and r_s are constant. R_{ee} is around 47 Å for bcn25 and 169 Å for β-casein, which is lower than the expected values from the zero model. The model values are calculated with a $K_r = 3.5$ and $\alpha = .57$, as obtained in section 2.1 for simulations of non-charged polymers with fixed bond lengths and $R_i/r_{eq} = .65$.

At 1 M, electrostatic interactions play only a minor role, but in these simulations the bond lengths vary around r_{eq}, and different amino acids have different radii with $\langle R_i \rangle / r_{eq} = .61$ for bcn25 and .64 for β-casein. Due to the smaller average residue size, smaller angles between the monomers are accessible and the average R_{ee} is smaller than expected.

If the ionic strength decreases, the shape effect of pH increases. At pH = pI the number of negatively and oppositely charged residues are equal. As oppositely charged particles attract each other, a decrease in R_{ee}, R_g and r_s are observed, corresponding to a compact and more Gaussian coil configuration.

When the particle charges up at pH $\neq$ pI, the influence of the same-signed charges, which repel each other, gets more important and R_{ee} and R_g increase. The shape factor increases, indicating a more rod-like configuration. These effects become gradually stronger with decreasing ionic strength.

The insets in Figure 5.5 show the probability distribution density for R_{ee}

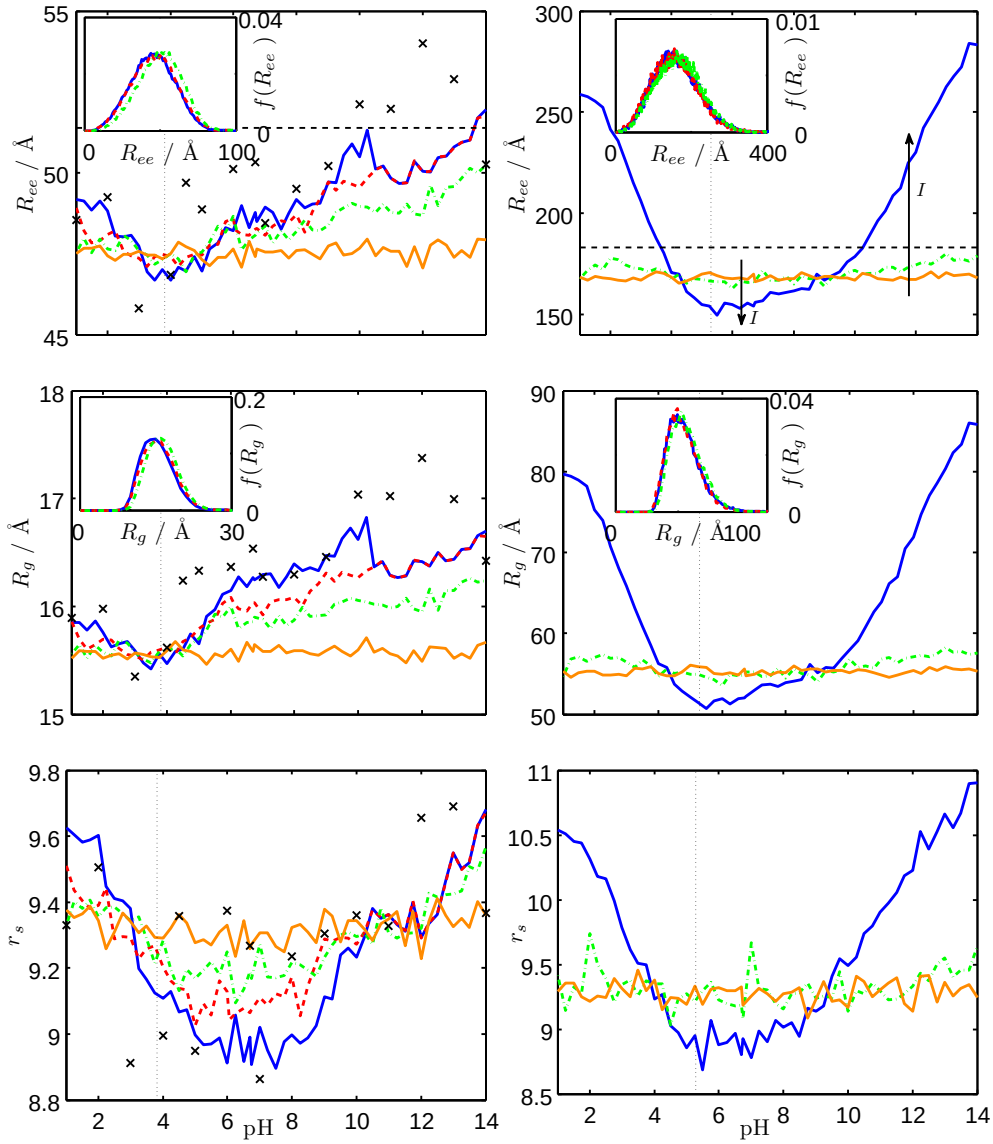

Figure 5.5: Root-mean-square end-to-end distance R_{ee} (top), rms radius of gyration R_g (middle) and shape ratio r_s (bottom) for bcn25 (left) and β-casein (right), as obtained from computer simulations with 30 mM explicit salt (×) and implicit salt of I/mM 0 (——), 30 (– –), 80 (– ·) and 10^3 (——). For R_{ee} a theoretical value was plotted from (2.4) with K_r=3.5 and α = .57 (– –). The insets show the probability distribution function for R_{ee} and R_g for the explicit salt 30 mM bcn25 simulation, and the implicit salt 80 mM β-casein simulation at pH 4 (——), 6.7 (– –) and 14 (– ·).

and R_g for the explicit salt bcn25 simulations at 30 mM and the implicit salt β-casein simulations at 80 mM at three different pH values. Both properties show fluctuations of the same order of magnitude as the mean value, and although the root mean square values have a significant dependence on pH, the actual distribution is practically constant upon changing pH at moderate ionic strengths.

These large configurational fluctuations make it time-consuming to obtain well-equilibrated averages. For the implicit salt simulations (performed with 100 times fewer steps, due to a much longer simulation time per step) the rough probability distribution indicates that the uncertainties for the root mean square values are still significant. This is also seen in the main plots, but the trends in the implicit and explicit case are identical.

The implicit salt simulations all show smooth property distributions, and smooth curves when the various properties are plotted against pH, which indicates converged simulations.

Finally, from the end-to-end distance distribution it is seen that β-casein needs a box larger than 375^3 Å^3 to make sure it does not interact with its image.

5.2 Adsorption on package material

5.2.1 Neutral surface

The entropic repulsion at a surface is investigated by introducing a neutral hard wall in the simulations of bcn25 and β-casein. From the distribution of the polymer mass centre as a function of the distance from the wall, the free energy was calculated using (2.13), see the blue lines in Figure 5.6. The mass centre distance from the wall is normalized with the bulk radius of gyration (16 Å and 54 Å) to compare the peptides, and both shape and onset of the repulsion are identical for bcn25 and β-casein.

The free energy at $z_{cm} \gg R_g$ is the bulk free energy, set to zero. At $z_{cm} < 2R_g$, the free energy increases, because the number of conformations is decreased by the excluded volume from the hard wall. Upon approaching the wall even more, the free energy increases up to 5 k_BT at 0.5 R_g for β-casein, corresponding to an $e^5 = 148$ higher polymer concentration in bulk, than at that distance from the wall. In the simulation, the polymer is therefore sampled much less close to the wall, and the resulting curve is noisy for $\beta\Delta A \gg 0$, while configurations corresponding to energies above $\sim$5 k_BT are not sampled at all.

The results from these protein-wall simulations are in good agreement with the free energy as predicted from the $z_{\max}$ distribution from bulk simulations (2.12). Note that, even though the number of Monte Carlo steps is ten times smaller in the bulk simulation, the fluctuations in the free energy curves are much less due to better sampling in bulk. In fact, for the bulk simulations, a smooth curve is obtained up to 13.5 k_BT (data not shown).

The free energy calculated from the Eisenriegler mass centre distribution (2.9) corresponds well to the β-casein repulsion. The repulsion for the much shorter bcn25 is overestimated, as seen before for small polymers in Figure 2.4.

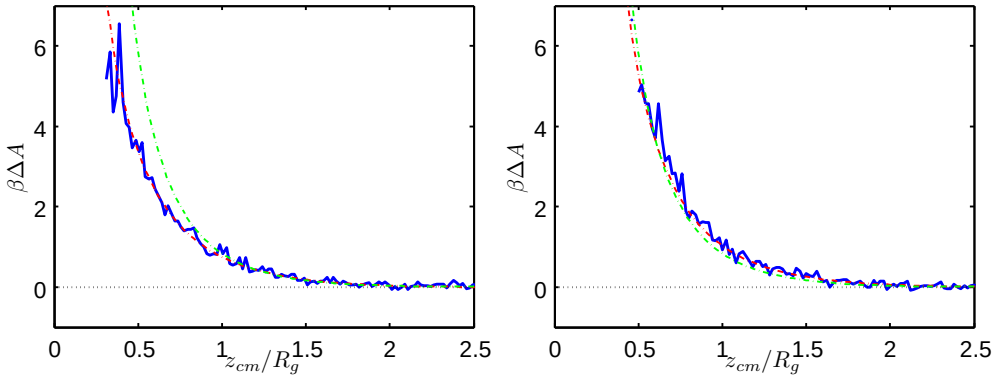

(a) bcn25 in 30 mM implicit salt

(b) β-casein in 80 mM implicit salt

Figure 5.6: Free energy, $\beta\Delta A$, as a function of the radius of gyration normalized distance between the mass centre and the wall, z_{cm}/R_g, at pH 4.50 and 80 mM implicit salt, as obtained from protein-wall simulations (—), as predicted from $z_{\max}$, sampled in bulk simulations (– ·), and as predicted from the zero model (– ·)

5.2.2 Negatively charged surface

Interactions with charged surface groups are investigated by introducing a Gouy-Chapman wall in the simulations. The resulting net peptide charges as a function of the distance from the wall is given in Figure 5.7 for bcn25 and β-casein.

Bcn25 has a bulk net charge of -2.4e at pH 4.5 (Figure 5.2) and is simulated near a positive wall. Upon approaching the wall, the peptide charge decreases to -4.8e in both implicit and explicit salt. Equation 3.39 describes the charge as a function of the distance from the wall, and the orange lines in Figure 5.7 are obtained by substituting the bulk charge and capacitance in this equation. Although the polymer is assumed to be a point charge in this equation, the range of the interaction is well estimated because the Debye screening and polymer size are in the same regime $\kappa^{-1} = 1.1R_g$, still, the shape of the prediction is somewhat off.

Better agreement with simulations is obtained by calculating the charge from (3.41), which takes the distribution of charges over the polymer into account. For the monomer distribution obtained from bulk simulations, (3.41) gives the green curve in Figure 5.7. Now, only at high charges, the prediction from bulk values deviates, because we assume the capacitance to be constant.

Finally, the magenta curve gives the prediction for a Gaussian monomer distribution with $\sigma = .6R_g$ and R_g, $\langle Z\rangle$ and C from the zero model. Here, the values for $\langle Z\rangle$ and C are overestimated, because the zero model does not take into account charge interactions which are still important at 30 mM, and the resulting curve lies lower.

β-casein is positively charged at pH 4.5, and upon approaching a negatively charged wall the charge increases from 5.5e to 8.0e at $z_{cm} = .3R_g$.

The calculation from the point charge assumption predicts a charge increase at $z_{cm} < R_g$, while in the simulation the increase is observed already at $z_{cm} \approx$

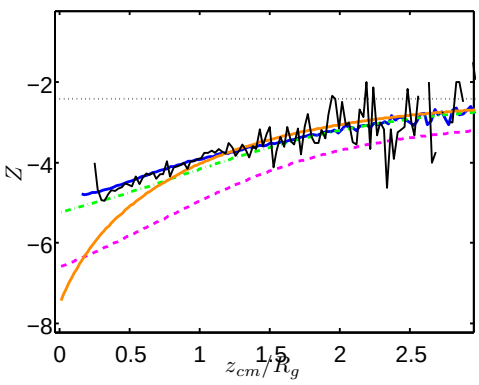

(a) bcn25 near a ρ=.5nm^{-2} wall, I=30 mM.

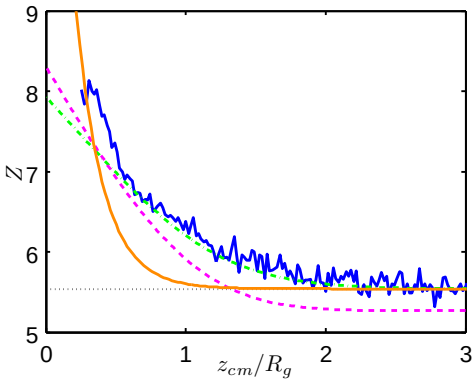

(b) β-casein near a ρ=-.5nm^{-2} wall, I=80 mM.

Figure 5.7: Net peptide charge, Z, as a function of the mass centre distance from a charged wall, z_{cm}/R_g, at pH 4.5, from polymer-wall simulations with implicit salt (—) and explicit salt (—), calculated using bulk simulation averages and (3.39) (—), calculated using bulk simulation averages and (3.41) (– ·) and calculated using the zero model and (3.41) (– –). The dashed black line indicates the charge in bulk simulations.

$2R_g$. For β-casein at 80 mM, R_g is much larger than the Debye screening length ($\kappa^{-1} = .2R_g$) and the point charge assumption clearly fails.

The integrated monomer distribution approach, however, describes the system better – both for bulk simulations as well as for the zero model, which in general describes the system better at higher ionic strengths, Equation (3.41) describes the charge behaviour well.

The influence of the oppositely charged wall on the free energy is seen in Figure 5.8, and both bcn25 and β-casein show an energy minimum at $z_{cm} \approx .5R_g$.

The electrostatic free energy as calculated from (3.42) from both bulk simulation results and from the zero model describes the initial energy decrease well, and the calculated total free energy, predicts the general shape and behaviour of the free energy.

For both β-casein and bcn25, however, the minimum is more shallow and at a larger distance from the wall than for the simulations, either because the repulsion is overestimated or the electrostatic interaction is underestimated. For the interaction between bcn25 and a hard wall, the repulsion was overestimated in the zero model case. Hence, the internal structure can be changed because of the charged wall, leading to an even softer repulsion.

The shift of the predicted minimum is more profound for β-casein at 80 mM, where the electrostatic term is less important due to screening. Furthermore, the steep increase in free energy for the simulation results of β-casein is seen closer to the wall, than the steep increase in the calculated repulsive term. Hence, probably the zero model fails due to an overestimation of the repulsion.

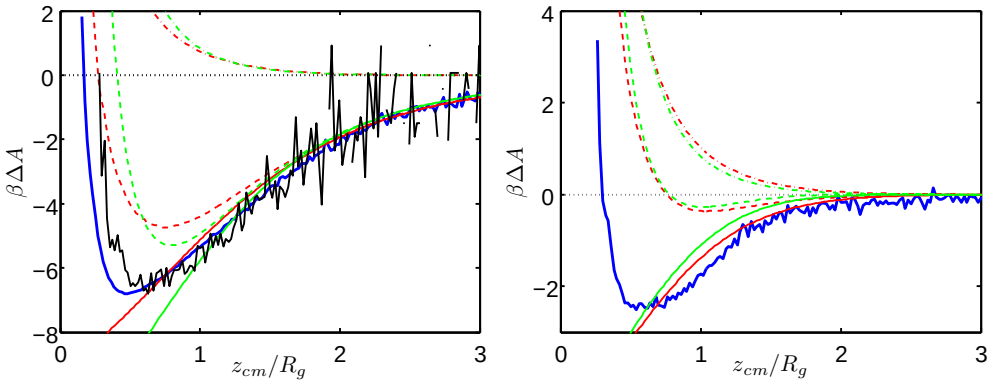

(a) bcn25 near a 200 Å^2 wall, I=30 mM (b) bcn25 near a -200 Å^2 wall, I=80 mM

Figure 5.8: Free energy, $\beta\Delta A$, as a function of the mass centre distance, z_{cm}/R_g, of β-casein from a charged wall at pH 4.5, from polymer-wall simulations with implicit salt (—) and explicit salt (—), and the repulsive (dashed-dotted line), electrostatic (dashed line) and total free energy (solid line), as calculated from bulk simulation results (red) and from the zero model (green).

5.2.3 Dependence on charge density

Figure 5.9 shows the peptide charge and free energy for β-casein near surfaces with varying charge densities.

At pH 4.5, β-casein is positively charged and the net charge increases upon approaching a negatively charged surface with a stronger increase for higher absolute charge densities. However, near a positively charged surface, the net charge decreases to reduce the electrostatic repulsion and again this effect is stronger near more highly charged surfaces.

For the free energy, the electrostatic contribution becomes more important upon increasing the charge density of a negatively charged wall. As a result, the free energy minimum becomes steeper and deeper by decreasing ρ from -0.50 nm^{-2} to -0.75 nm^{-2}, while no minimum is seen for $\rho = -0.25$ nm^{-2}. Because of the deep minimum for the highest charged wall, the probability of finding the peptide at distances far from the wall is very small, giving bad sampling of Z and ΔG at $z_{cm} \gg R_g$, still, both fluctuate around the bulk mean values.

Remarkably, for the positively charged wall there is also a free energy minimum, and even though β-casein is positively charged in bulk at this pH, this becomes deeper upon increasing the charge density. As seen in Figure 5.9, the peptide adapts its charge to its environment, leading to less electrostatic repulsion, but even for the highest charged case the charge is about $3e$ at the free energy minimum of -2 k_BT. Note also the shape difference of the free energy curves; near a positively charged wall a broader minimum at a larger protein-wall separation is observed.

The dependence of the radius of gyration and the root mean square z-component of R_g, $R_{g,z}$ on the mass centre distance from the wall gives an indication of what explains this behaviour, see Figure 5.10. At high protein-wall distances both properties go to their bulk value, which is found at $.7R_g$ for

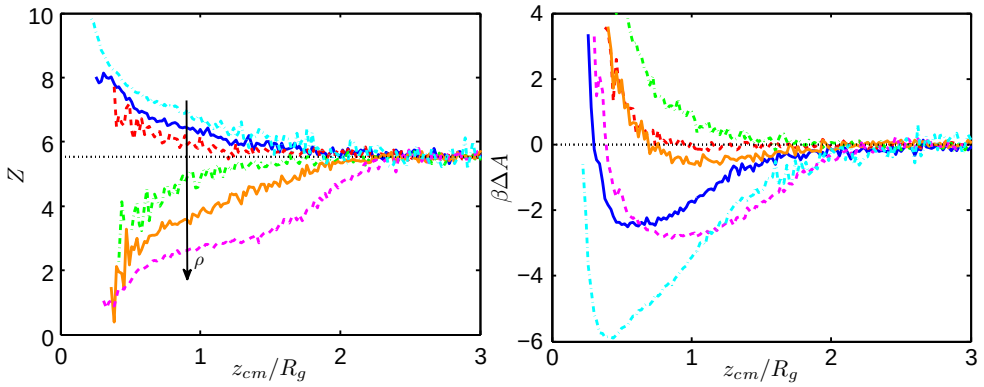

Figure 5.9: Net β-casein charge, Z (left), and free energy, $\beta\Delta A$ (right), at pH 4.5 and $I = 80$ mM as a function of the mass centre distance, z_{cm}/R_g, from a charged wall with ρ/nm^{-2} =-0.75 (– ·), -0.50 (—), -0.25 (– –), 0.25 (– ·), 0.5 (—) and 0.75 (– –).

$R_{g,z}$, and near a wall with a low charge density, $R_{g,z}$ decreases because of the excluded volume. After an initial decrease in R_g, a strong increase is seen for $z_{cm} < R_g$, as the peptide stretches itself in the x and y-direction on the surface.

Near a highly charged positive wall, however, $R_{g,z}$ increases before it approaches the low charged wall values at close separation. The stretching of the polymer in the z-direction leads to an increase in R_g too, which is smaller than for $R_{g,z}$, because $R_{g,x}$ and $R_{g,y}$ are constant in this regime (data not shown). Near the negatively charged wall with an equally strong free energy minimum, the polymer stretches only slightly, and no dramatic increase in $R_{g,z}$ is seen.

The normalized, logarithmic probability per residue as a function of the residue-wall distance, $-\beta \ln g(z_i)$, gives the effective residue free energy, which – since they are linked together – also depends on the other residues. Contour plots for this free energy near the positively and negatively charged wall of Figure 5.10 show a completely different behaviour for both cases, see Figure 5.11. Near a negatively charged wall, a deep minimum near residue 121 and several other minima throughout the peptide are seen, corresponding to the left simulation snapshot, where different regions in the middle part of the peptide are adsorbed.

Near a positively charged wall, the absolute minimum is at residue 58, and large regions in the beginning of the peptide show strong adsorption, including the negatively charged bcn25 part from residue 16 to 41. This corresponds to the right simulation snapshot, where the head group is adsorbed and the tail stretches out in the solution. For the white regions no value could be calculated, because the free energy was too high to be sampled.

Comparing the two contour plots more closely, we see that parts which show deep minima in one case, show high values in the other, because regions dominated by acidic groups, like the bcn25 part, are electrostatically attracted to positively charged surfaces, but repelled by negatively charged surfaces, and vice versa for basic regions.

Electrostatic interactions last on a length scale corresponding to κ^{-1}, which

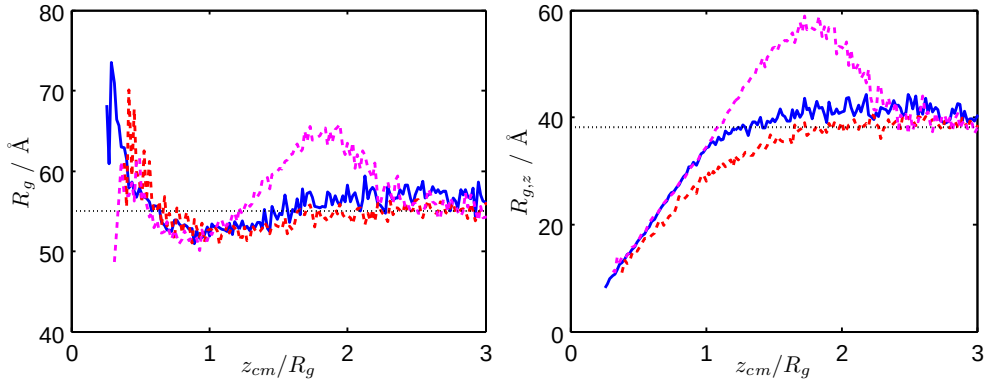

Figure 5.10: Radius of gyration, R_g (left), and its z-component, $R_{g,z}$ (right), for β-casein as a function of its mass centre distance z_{cm}/R_g from a charged wall with ρ/nm^{-2} = -0.50 (—), -0.25 (– –) and 0.75 (– –) at pH 4.5 and $I = 80$ mM. The dashed black lines indicate bulk averages.

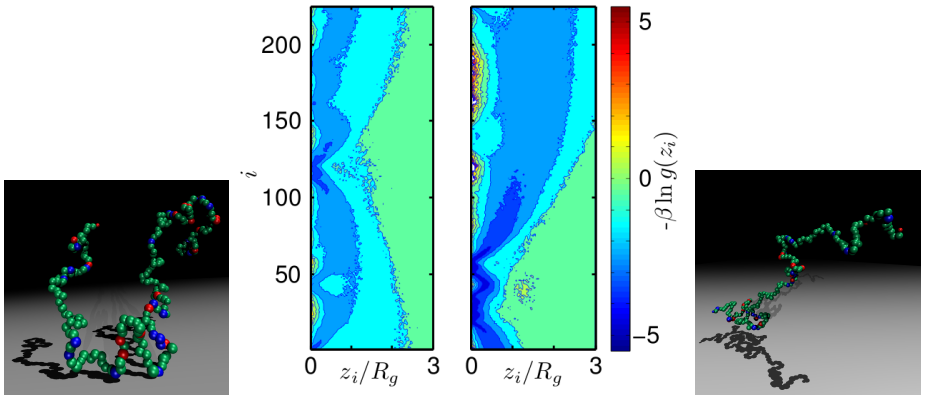

Figure 5.11: Contour plot of the logarithmic, normalized probability per residue i as a function of the residue distance from the wall, $-\beta \ln g(z_i)$, and snapshots for the adsorbed peptides at pH 4.5 and $I = 80$ mM for β-casein near a charged wall with ρ/nm^{-2} = -0.50 (left) and 0.75 (right).

is here $.2R_g$, and indeed the strong free energy minima and maxima are seen only for small residue-wall separations. However, the amino acids form a linked chain, and hence even at $z_i > .2R_g$ peptide-wall interactions have an influence on the probability distribution of residues. When a small region of the peptide is strongly adsorbed to the wall, while the rest is not, the peptide behaves as a grafted polymer of which one monomer is bound to a surface.

From Figure 5.10 and 5.11, the observed behaviour of the peptide adsorption free energy in Figure 5.9 (right) can thus be understood. Because of its amphiphilic character and its ability to change the net charge, β-casein can adsorb on both negatively and positively charged surfaces. Near a negatively charged surface, residues from different parts of the protein are attracted to the wall, giving a deep and steep free energy minimum. Upon approaching a positively charged surface, the peptide stretches, so that the negatively charged part is adsorbed to the wall, while the tail is in the solution. The polymer thus behaves as a grafted polymer, with a free energy minimum at larger distances.

The different adsorption mechanisms also explains the difference in the net charge dependence on the polymer mass centre distance from the wall for ρ/nm^{-2} -.75 and .75, see Figure 5.9 (left). Upon approaching the negatively charged wall, the net charge gradually increases as the peptide becomes more titrated. Upon approaching the positively charged wall, however, the net charge drops much steeper at relatively high protein-wall distances, and decreases less steep closer to the wall. This is because the observed net charge drop near the positively charged wall is caused mainly by adsorption of the head group, occurring at relative long mass centre distances from the wall.

5.2.4 Hydrophobic charged surface

In Figure 5.12a, a hydrophobic attraction between the charged surface and hydrophobic residues of β-casein is introduced. Upon increasing the strength of this attraction, $\epsilon_{\mathrm{phob},is}$, both hydrophobic and electrostatic interactions contribute to the attraction, and the free energy minimum becomes deeper and closer to the wall. The range of the interaction and the position of the repulsion onset are however not influenced, and the net charge as a function of the distance is the same in all cases.

5.2.5 Dependence on pH

The influence of pH on the interaction between β-casein and a negatively charged surface is shown in Figure 5.12b. Upon increasing pH to the isoelectric point at 5.5, the bulk peptide charge is zero, and the capacitance is in a local minimum, see Figures 5.2 and 5.4. Hence, the peptide charge can only increase slightly and only a small free energy minimum is observed.

At normal milk pH, the peptide is negatively charged and thus repelled from the negatively charged surface. This corresponds well with the observation that normal milk, although more complex, does not adhere much too surfaces.

5.2.6 Effect of charge regulation

In all above presented results, the net peptide charge adapts to the environment, and the influence thereof on the free energy is investigated by setting the indi-

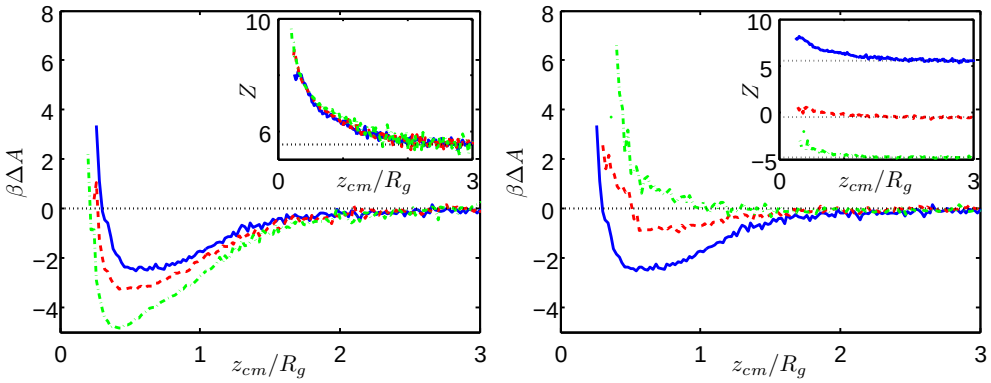

(a) Interaction with a surface with hydrophobicity, $\epsilon_{\mathrm{phob},is}$=0 (—), .25 (– –) and .5 (– ·) at pH 4.5.

(b) Interaction with a non-hydrophic surface at pH 4.5 (—), pH 5.5 (– –) and pH 6.7 (– ·).

Figure 5.12: Free energy, $\beta\Delta A$, and net peptide charge, Z (inset), for β-casein at $I = 80$ mM as a function of the mass centre distance, z_{cm}/R_g, from a charged wall with ρ/nm^{-2} = -0.50.

vidual monomer charges to their bulk mean values and keeping them constant during the simulation, see Figure 5.13a.

The net peptide charge is constant as a function of the polymer-wall distance and near a -0.50 nm^{-2} surface, the free energy minimum is less deep. The change in the free energy minimum, 0.4 k_BT, corresponds to the contribution from charge regulation.

Near the 0.75 nm^{-2} surface, no net attraction is seen without charge regulation. Charge regulation is thus crucial for the initially positively charged β-casein, to adsorb on a positively charged surface.

5.2.7 Effect of point mutation

The absolute minimum in $-\beta \ln g(z_i)$ in Figure 5.11 (left), was at residue 121, a basic lysine amino acid (K), and the effect of a point mutation at this position to the neutral and equally sized methionine (M) is presented in Figure 5.13b.

The net peptide charge as a function of the polymer distance from the wall is shifted with $1e$, as the number of basic sites is reduced with one. The resulting free energy minimum is only half as deep, with a change from around -2.5 k_BT to -1.5 k_BT.

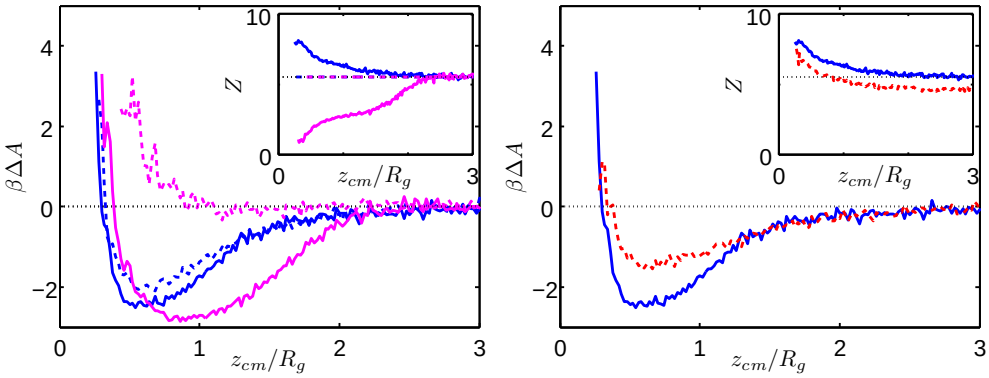

(a) β-casein near a wall with ρ/nm^{-2} = -0.50 (blue) and .75 (magenta), and with titratable residues (solid lines) and residues constant at their bulk mean charge (dashed lines)

(b) β-casein (—) and β-casein point mutated at 121 with K $\rightarrow$ M (– –) near a wall with ρ/nm^{-2} = -0.50.

Figure 5.13: Free energy, $\beta\Delta A$, and net peptide charge, Z (inset), at pH 4.5 and I = 80 mM as a function of the mass centre distance, z_{cm}/R_g, from a charged wall.

Chapter 6

Discussion

In this work, the interaction between single, coarse grained β-casein peptides and simple surfaces is investigated on a nanometre scale, to get an idea of the molecular origin of the macroscopic observation that fermented milk sticks to its package. This approach, the developed model, the data analysis are discussed here.

The interaction of fermented milk with package materials is of course much more complex than in our model. Fermented milk consists of a range of different molecules, which possibly interact with the package material, and this gives, moreover, rise to potential cooperation or competition effects in surface adsorption. Furthermore, adsorption is a time-dependent process and the Monte Carlo results provide only equilibrium properties. Finally, the different components also interact with each other, giving rise to effects on a macroscopic scale, like a high viscosity and a thick adsorbed layer on package material.

Experimental data [7] indicates, however, that proteins are very important for the fermented milk adsorption in the equilibrium state, and that equilibrium is obtained after 80 to 170 h, the time scale for distribution and consuming packages. The most abundant protein in fermented milk is β-casein, so the adsorption of individual β-casein provides important insight in the microscopic adsorption of the first layer, which is a crucial first step to full understanding of adsorption of a fermented milk gel.

For the surface, the charge density and microscopic hydrophobicity parameters are unknown, and inhomogeneity of the surface properties and roughness is not taken into account in the model. The here presented results, however, show the trends in the polymer-surface interactions upon changing the charge density and hydrophobicity. Furthermore, the exact value of the charge density and hydrophobic interaction energy do not change the general mechanisms for adsorption as described here.

Finally, casein adsorption plays also a role in other problems like fouling, and by investigating general processes, data has been obtained, which can provide more understanding in these fields too.

The coarse grained model, as developed in chapter 3, is based on many parameters and simplifications of which most are verified with experimental data or full atomistic simulations, either in this work or in cited sources.

The range and strength of hydrophobic interactions, however, are estimated from chemical intuition and should be obtained form full atomistic simulations to obtain more reliable results.

Furthermore, there is no constraint on the angles between neighbouring residues, other than a lower boundary, because residues can not overlap. The angular distribution and thus R_g and R_{ee} are therefore likely to be overestimated, which probably leads to a higher entropic repulsion in the simulations. However, this is partly compensated for since the equilibrium distance between monomers is overestimated, because values from crystal structures of folded proteins are used, which are more compact than unstructured proteins.

The influence of these approximations is however not expected to be of major importance on the general behaviour. More experimental data to compare the obtained values for the size and charge of the peptide with, however, would give a stronger foundation for the drawn conclusions.

The equilibration time (with time, the number of Monte Carlo steps) is estimated from the time-averaged fluctuations in the various properties. The property - time dependence during the first Monte Carlo steps, however, would have been a better indicator to verify, after how many steps, equilibrium has been reached and the observed properties fluctuate around an equilibrium value.

Furthermore, from the time dependence, correlation times could have been obtained, to make sure properties are sampled independently, making the calculation of error bars possible. Smooth curves are however obtained for most properties and trends can be explained by theory, indicating good quality data for drawing conclusions about the general principles.

Chapter 7

Conclusion

On a supramolecular level, fermented milk is a sophisticated viscous gel of colloidal proteins and fat particles, making the adhesion of fermented milk on packaging materials a complex problem. This study shows that even on a single β-casein peptide level, many different interactions result in complex polymer-surface attraction.

To study β-casein adsorption on surfaces, a coarse grained model with interactions which are sensitive to implicit salt and water is developed and verified with data from experiments as well as computer simulations. Good agreement between models with implicit salt and explicit salt particles is seen, and bulk simulations show a strong salt and pH dependence of peptide properties. Furthermore, most trends in the simulation results can be explained by the here assembled theoretical zero model, but the model fails to rightly predict the deepness of the free energy minimum for larger peptides, probably due to an overestimation of the repulsion.

β-casein is an amphiphilic, unstructured molecule, and is attracted by both polar and hydrophobic surfaces. Moreover, because of its high capacitance at the pH of fermented milk, the residue charges adapt to their environment, and β-casein acts as a molecular chameleon. Near negatively charged surfaces, the peptide is highly positively charged and spreads out on the surface upon adsorption. Near positively charged surfaces, the net charge becomes almost neutral, and the negatively charged head group adsorbs on the surface, while the tail stretches out in the solution. For hydrophobic surfaces with negative groups, a model surface for materials used in packaging, the combined effect of hydrophobic and electrostatic interactions leads to an even stronger adsorption.

The results indicate that small perturbations of the system, like a point mutation, the absence of charge regulation, or a pH increase have a significant effect on the attraction. At the pH of normal milk, for example, no adsorption on the charged reference surface is seen, which agrees well with the observation that normal milk does not adhere as much to packages.

Due to the high dependence of the peptide-surface interaction on surface properties, changing the surface has a clear effect on the adsorption, which is promising for finding non-sticky materials. Because of the many interaction mechanisms of β-casein, and the numerous different molecules in and the viscosity of fermented milk, however, the product is likely to adhere in any case, but the amount of adsorbed material could be decreased.

Chapter 8

Suggestions for further research

Here, some ideas for future research are discussed, with focus on how the model system can be improved, further verified, and what other simulation studies could be performed. A discussion on possible experimental research on the adhesion of fermented milk can be found elsewhere [7].

Experimental studies and computer simulations using other techniques on the here studied bulk properties of β-casein as a function of salt and pH could be performed to verify the presented simulation results, and therewith the developed model. From titration experiments on pure β-casein both the charge and capacitance as a function of pH and salt can be obtained, and using CD spectroscopy, NMR, and SAXS, its shape and size can be studied. Classical density functional theory (DFT) is a theoretical framework and can be used to verify the here used simulation method using the same model.

From atomistic molecular dynamics simulations, the chosen parameters for R_i, $\epsilon_{\text{phob},ij}$, r_{phob}, r_{eq}, k, k, and $\epsilon_{\text{phob},is}$ can be verified for unstructured proteins, and possibly improved. Furthermore, the distribution of the angles between three neighbouring monomers can be used to restrict these in the simulation.

Here, only simple hydrophobic and charged surface have been investigated, the interaction between more advanced materials, with non-stick properties, like zwitterionic surfaces and polymer brushes, can be an interesting next step.

In the for this study written simulation program, multiple peptides can be simulated to study the interactions between β-casein peptides, and possible cooperation or competition effects upon surface adsorption.

The interaction between casein micelles and packaging material can be studied using a further coarse grained model. The micelles are covered with κ-casein, and the interaction potential between a κ-casein brush and packaging material can be used to obtain the potential for the micelle-surface interaction.

Finally, the zero model can be used to give fast and, it seems, good predictions for short peptides. Due to the speedy coarse grained model, a (possible web) interface can be designed which predicts the free energy curves, and charge and shape behaviour near a given surface, from a given amino acid sequence. This can even be extended to a full 3D free energy landscape as a function of pH, ionic strength and charge density. However, for this more testing and

comparison between the model and different peptides needs to be done.

Chapter 9

Acknowledgement

Finally, I would like to gratefully thank: my supervisors Thorbjörn Andersson, Mikael Lund and Marie Skepö, for their help, suggestions and being a great source of inspiration; everybody I've discussed sticky filmjölk with the past half year, and especially Jan Forsman, Kristina Hansson, Per Linse and Torbjörn Åkeson, for their fresh ideas; SuMo Biomaterials, for giving the opportunity to present and discuss this work at one of their meetings; Lunarc, for providing computer time; and finally my colleges at Theoretical Chemistry and at Tetra Pak, for discussions, friendship and support.

References

[1] Law, A. Effects of heat treatment and acidification on the dissociation of bovine casein micelles. *Journal of Dairy Research* **63**, 35–48 (1996). URL http://dx.doi.org/10.1017/S0022029900031526.

[2] Walstra, P. *Dairy Chemistry and Physics* (Wiley-Interscience, 1984).

[3] Tuinier, R. & De Kruif, C. Stability of casein micelles in milk. *Journal of Chemical Physics* **117**, 1290–1295 (2002). URL http://link.aip.org/link/doi/10.1063/1.1484379.

[4] Eurostat, apro_mk_farm. URL http://appsso.eurostat.ec.europa.eu/nui/show.do?query=BOOKMARK_DS-052668_QID_623AFFCB_UID_-3F171EB0&layout=TIME,C,X,0;GEO,L,Y,0;PRODMILK,L,Z,0;MILKITEM,L,Z,1;INDICATORS,C,Z,2;&zSelection=DS-052668INDICATORS,OBS_FLAG;DS-052668MILKITEM,PRO;DS-052668PRODMILK,COWYI;&rankName1=TIME_1_0_0_0&rankName2=PRODMILK_1_2_-1_2&rankName3=MILKITEM_1_2_-1_2&rankName4=INDICATORS_1_2_-1_2&rankName5=GEO_1_2_0_1&pprRK=FIRST&pprSO=PROTOCOL&ppcRK=FIRST&ppcSO=ASC&sortC=ASC_-1_FIRST&rStp=&cStp=&rDCh=&cDCh=&rDM=true&cDM=true&footnes=false&empty=false&wai=false&time_mode=NONE&lang=EN&cfo=%23%23%23.%23%23%23%2C%23%23%23.

[5] Gaucheron, F. The minerals of milk. *Reproduction Nutrition Development* **45**, 473–484 (2005). URL http://dx.doi.org/10.1051/rnd:2005030.

[6] Atkinson, S., Alston-Mills, B., Lönnerdal, B. & Neville, M. Major minerals and ionic constituents of human and bovine milks. *Handbook of Milk Composition (Jensen, RG, ed.). Academic Press, Inc., San Diego, CA* 593–622 (1995).

[7] Hansson, K. *Why do Fermented Milk Products Stick to Packaging Material Surfaces*. Master's thesis, Linköping University (2011). URL http://urn.kb.se/resolve?urn=urn:nbn:se:liu:diva-68877.

[8] Jeurnink, T., Walstra, P. & De Kruif, C. Mechanisms of fouling in dairy processing. *Nederlands Melk- en Zuiveltijdschrift* **50**, 407–426 (1996).

[9] Holt, C., Wahlgren, N. & Drakenberg, T. Ability of a beta-casein phosphopeptide to modulate the precipitation of calcium phosphate by forming amorphous dicalcium phosphate nanoclusters. *Biochemical Journal* **314**,

1035–1039 (1996). URL https://www.ncbi.nlm.nih.gov/pmc/articles/PMC1217110/.

[10] Eurostat, apro_mk_pobta. URL http://appsso.eurostat.ec.europa.eu/nui/show.do?query=BOOKMARK_DS-052400_QID_-1CAC4657_UID_-3F171EB0&layout=TIME,C,X,0;GEO,L,Y,0;PRODMILK,L,Z,0;MILKITEM,L,Z,1;INDICATORS,C,Z,2;&zSelection=DS-052400PRODMILK,MC140;DS-052400MILKITEM,PRO;DS-052400INDICATORS,OBS_FLAG;&rankName1=TIME_1_0_0_0&rankName2=PRODMILK_1_2_-1_2&rankName3=MILKITEM_1_2_-1_2&rankName4=INDICATORS_1_2_-1_2&rankName5=GEO_1_2_0_1&pprRK=FIRST&pprSO=CUSTOM&ppcRK=FIRST&ppcSO=ASC&sortC=ASC_-1_FIRST&rStp=&cStp=&rDCh=&cDCh=&rDM=true&cDM=true&footnes=false&empty=false&wai=false&time_mode=NONE&lang=EN&cfo=%23%23%23.%23%23%23%2C%23%23%23.

[11] Tetra pak (retreived 29 Aug. 2011). URL www.tetrapak.com.

[12] Dunker, A., Brown, C., Lawson, J., Iakoucheva, L. & Obradovic, Z. Intrinsic disorder and protein function. *Biochemistry* **41**, 6573–6582 (2002). URL http://dx.doi.org/10.1021/bi012159.

[13] Tompa, P. Intrinsically unstructured proteins. *Trends in Biochemical Sciences* **27**, 527–533 (2002). URL http://dx.doi.org/10.1016/S0968-0004(02)02169-2.

[14] Evans, D. & Wennerström, H. *The Colloidal Domain: Where Physics, Chemistry, and Biology Meet* (Wiley-VCH, 1999).

[15] Lund, M. & Jönsson, B. On the charge regulation of proteins. *Biochemistry* **44**, 5722–5727 (2005). URL http://dx.doi.org/10.1021/bi047630o.

[16] Lund, M. Electrostatic chameleons in biological systems. *Journal of the American Chemical Society* (2010). URL http://dx.doi.org/10.1021/ja106480a.

[17] Clisby, N. Accurate estimate of the critical exponent ν for self-avoiding walks via a fast implementation of the pivot algorithm. *Physical Review Letters* **104**, 055702 (2010). URL http://dx.doi.org/10.1103/PhysRevLett.104.055702.

[18] Eisenriegler, E. & Maassen, R. Center-of-mass distribution of a polymer near a repulsive wall. *Journal of Chemical Physics* **116**, 449–450 (2002). URL http://dx.doi.org/10.1063/1.1423323.

[19] Emboss isoelectric point calculator. URL http://emboss.open-bio.org/wiki/Appdoc:Iep#Data_files.

[20] DeLoura, M. Game programming gems 2. *Charles River Media* (2001).

[21] Monticelli, L. *et al.* The martini coarse-grained force field: extension to proteins. *Journal of Chemical Theory and Computation* **4**, 819–834 (2008). URL http://dx.doi.org/10.1021/ct700324x.

[22] Fischer, H., Polikarpov, I. & Craievich, A. Average protein density is a molecular-weight-dependent function. *Protein Science* **13**, 2825–2828 (2004). URL http://dx.doi.org/10.1110/ps.04688204.

[23] Eisenberg, D., Weiss, R., Terwilliger, T. & Wilcox, W. Hydrophobic moments and protein structure. *Faraday Symposia of the Chemical Society* **17**, 109–120 (1982). URL http://dx.doi.org/10.1039/FS9821700109.

[24] Chrysina, E., Brew, K. & Acharya, K. Crystal structures of apo-and holobovine α-lactalbumin at 2.2-å resolution reveal an effect of calcium on interlobe interactions. *Journal of Biological Chemistry* **275**, 37021 (2000). URL http://dx.doi.org/10.1074/jbc.M004752200.

[25] Brownlow, S. *et al.* Bovine β-lactoglobulin at 1.8 å resolution — still an enigmatic lipocalin. *Structure* **5**, 481–495 (1997). URL http://dx.doi.org/10.1016/S0969-2126(97)00205-0.

[26] Moore, S., Anderson, B., Groom, C., Haridas, M. & Baker, E. Three-dimensional structure of diferric bovine lactoferrin at 2.8 å resolution. *Journal of molecular biology* **274**, 222–236 (1997). URL http://dx.doi.org/10.1006/jmbi.1997.1386.

[27] Becker, J. & Reeke, G. Three-dimensional structure of beta 2-microglobulin. *Proceedings of the National Academy of Sciences* **82**, 4225–4229 (1985). URL http://www.pnas.org/content/82/12/4225.

[28] Adachi, M. *et al.* Crystal structure of soybean 11s globulin: glycinin a3b4 homohexamer. *Proceedings of the National Academy of Sciences* **100**, 7395–7400 (2003). URL http://dx.doi.org/10.1073/pnas.0832158100.

[29] Riley, K., Hobson, M. & Bence, S. *Mathematical Methods for Physics and Engineering* (Cambridge Univ Pr, 2006).

[30] Trulsson, M. *Simulations of Simple Fluids and Surface Forces*. Ph.D. thesis, Lund University (2011).

[31] Frenkel, D. & Smit, B. *Understanding Molecular Simulation: From Algorithms to Applications*, vol. 1 (Academic Press, 2002).

[32] Lund, M., Trulsson, M. & Persson, B. Faunus: An object oriented framework for molecular simulation. *Source Code for Biology and Medicine* **3** (2008). URL http://dx.doi.org/10.1186/1751-0473-3-1.

[33] Bonsing, J., Ring, J., Stewart, A. & Mackinlay, A. Complete nucleotide sequence of the bovine beta-casein gene. *Australian Journal of Biological Sciences* **41**, 527–537 (1988). URL http://www.ncbi.nlm.nih.gov/pubmed/3271384.

Appendix A

Input Files

2011-08-30 bcn25.mol2 1

```
@<TRIPOS>MOLECULE
*****
 27 26 0 0 0
SMALL
GASTEIGER
Energy = 0
# Matlab generated based on holt1996ability RELEELNVPGEIVESLSSSEESITR
@<TRIPOS>ATOM
       1       F       1      -1       4       F       1     NTR       0       #  N-term
       2       F       2      -3      -1       F       2     ARG       0       #       R
       3       F       3       4      -1       F       3     GLU      -1       #       E
       4       F       4      -1      -3       F       4     LEU       0       #       L
       5       F       5       4      -2       F       5     GLU      -1       #       E
       6       F       6      -1       4       F       6     GLU      -1       #       E
       7       F       7       0       1       F       7     LEU       0       #       L
       8       F       8       1       2       F       8     ASN       0       #       N
       9       F       9      -3       1       F       9     VAL       0       #       V
      10       F      10      -3       3       F      10     PRO       0       #       P
      11       F      11      -1       3       F      11     GLY       0       #       G
      12       F      12      -2       1       F      12     GLU      -1       #       E
      13       F      13       4      -3       F      13     ILE       0       #       I
      14       F      14      -3      -3       F      14     VAL       0       #       V
      15       F      15       2       1       F      15     GLU      -1       #       E
      16       F      16      -3       3       F      16     SER       0       #       S
      17       F      17       1      -3       F      17     LEU       0       #       L
      18       F      18      -3      -2       F      18     SER       0       #       S
      19       F      19       3      -3       F      19     SER       0       #       S
      20       F      20      -2      -2       F      20     SER       0       #       S
      21       F      21      -3       3       F      21     GLU      -1       #       E
      22       F      22       2       2       F      22     GLU      -1       #       E
      23       F      23       2       1       F      23     SER       0       #       S
      24       F      24      -1       2       F      24     ILE       0       #       I
      25       F      25      -3      -2       F      25     THR       0       #       T
      26       F      26      -3       4       F      26     ARG       0       #       R
      27       F      27       4      -3       F      27     CTR      -1       #  C-term
@<TRIPOS>BOND
1 1 2 1
2 2 3 1
3 3 4 1
4 4 5 1
5 5 6 1
6 6 7 1
7 7 8 1
8 8 9 1
9 9 10 1
10 10 11 1
11 11 12 1
12 12 13 1
13 13 14 1
14 14 15 1
15 15 16 1
16 16 17 1
```

```
## Implicit titration processes; http://emboss.open-bio.org/wiki/Appdoc:Iep#Data_files
Process  HASP  ASP  3.9  4.50
Process  HCTR  CTR  3.6  4.50
Process  HGLU  GLU  4.1  4.50
Process  HHIS  HIS  6.5  4.50
Process  HNTR  NTR  8.6  4.50
Process  HTYR  TYR  10.1 4.50
Process  HLYS  LYS  10.8 4.50
Process  HCYS  CYS  8.5  4.50
Process  HARG  ARG  12.5 4.50
```



```
# ------------------------------------------------------------
#   Faunus atom parameters
#    Chris Evers
#    Lund, 28-Jul-2011
#    With \rho = 1.41
#    Format:
#     name   charge radius eps    Mw     pKa   hydrophobic
#             (e)    (Å)   (kT)  (g/mol)
# ------------------------------------------------------------

# Amino Acids:
Atom  ALA      0     2.7    0.1     71     0.0    yes
Atom  ARG      0     3.5    0.1    156    12.5    no
Atom  ASN      0     3.2    0.1    114     0.0    no
Atom  ASP     -1     3.2    0.1    115     3.9    no
Atom  CYS     -1     3.1    0.1    103     8.5    no
Atom  GLN      0     3.3    0.1    128     0.0    no
Atom  GLU     -1     3.3    0.1    129     4.1    no
Atom  GLY      0     2.5    0.1     57     0.0    no
Atom  HIS      0     3.4    0.1    137     6.5    no
Atom  ILE      0     3.2    0.1    113     0.0    yes
Atom  LEU      0     3.2    0.1    113     0.0    yes
Atom  LYS      0     3.3    0.1    128    10.8    no
Atom  MET      0     3.3    0.1    131     0.0    yes
Atom  PHE      0     3.5    0.1    147     0.0    yes
Atom  PRO      0     3.0    0.1     97     0.0    yes
Atom  SER      0     2.9    0.1     87     0.0    no
Atom  THR      0     3.1    0.1    101     0.0    no
Atom  TRP      0     3.7    0.1    186     0.0    yes
Atom  TYR     -1     3.6    0.1    163    10.1    no
Atom  VAL      0     3.0    0.1     99     0.0    yes
Atom  CTR     -1     1.7    0.1     17     3.6    no
Atom  NTR      0     0.7    0.1      1     8.6    no
Atom  HARG     1     3.5    0.1    156    12.5    no
Atom  HASP     0     3.2    0.1    115     3.9    no
Atom  HCYS     0     3.1    0.1    103     8.5    no
Atom  HGLU     0     3.3    0.1    129     4.1    no
Atom  HHIS     1     3.4    0.1    137     6.5    no
Atom  HLYS     1     3.3    0.1    128    10.8    no
Atom  HTYR     0     3.6    0.1    163    10.1    no
Atom  HCTR     0     1.7    0.1     17     3.6    no
Atom  HNTR     1     0.7    0.1      1     8.6    no

# Other particles:
Atom  ghost    0     0.000001 0    0.000001 0.0   no
Atom  NA      +1     2.0    0.2179 1       0.0    no
Atom  CL      -1     2.0    0.1689 1       0.0    no
Atom  ANp     -1     1e-4   0.1    1       0.0    no
```

```
################################################
## Input file for wpDH
##
## Chris Evers
## Lund, 28 july 2011
################################################

# Simulation
  macrosteps            10
  microsteps            100000
  write_files           yes         # write output files to disk
  traj_runfrac          0.0005      # write out trajectory once every 1/traj_runfrac steps

# Container
  cuboid_xlen           1000        # length of simulation box in x-direction [Å]
  cuboid_ylen           1000        # length of simulation box in y-direction [Å]
  cuboid_zlen           1000        # length of simulation box in z-direction [Å]
  cuboid_xmin           0           # minimum position of mass center in x-direction [Å]
  cuboid_ymin           0           # minimum position of mass center in y-direction [Å]
  cuboid_zmin           0           # minimum position of mass center in z-direction [Å]
  cuboid_xmax           1000        # maximum position of mass center in x-direction [Å]
  cuboid_ymax           1000        # maximum position of mass center in y-direction [Å]
  cuboid_zmax           1000        # maximum position of mass center in z-direction [Å]

# Polymer
  polymer               bcn224.mol2 # polymer residues and connectivity
  atomfile              faunatoms.in # particle properties # faunatoms_rho.9.in #
  pol_num               1           # number of polymers
  pol_ends              1           # polymer ends in Ree calculations
                                    # pol_ends=1: ignore first and last particle

# Moves
  monomer_runfrac       1           # monomer translation runfraction
  monomer_dp            6           # displacement parameter [Å]

  moltrans_runfrac      1           # molecular translation runfraction
  moltrans_dp           59          # displacement parameter [Å]

  molrot_runfrac        1           # molecular rotation runfraction
  molrot_dp             3           # displacement parameter [degrees]

  crankshaft_runfrac    1           # crankshaft move runfraction
  crankshaft_dp         36          # displacement parameter [degrees]

  branchrot_runfrac     1           # branch rotation runfraction
  branchrot_dp          11          # displacement parameter [degrees]

  eqtit_runfrac         1           # titration runfraction
  eqtit_processes       eq.in       # titration processes
  pol_charges           q.in        # read monomer charges if eqtit_runfrac=0

# Interaction parameters
  lj_epsilon            .2          # pauli repulsion interaction parameter

  harmonic_k            0.76        # harmonic bond force constant [kT Å-2]
  harmonic_req          4.9         # harmonic bond equilibrium distance [Å]

  pairphob_u            -.5         # hydrophobic pair interaction energy [kT]
  pairphob_r            3.0         # hydrophobic pair interaction distance [Å]
  wallphob_u            -.5         # hydrophobic wall interaction energy [kT]
  wallphob_r            3.0         # hydrophobic wall interaction distance [Å]

  pH                    6.70        # pH
  ionicstr              .080        # Ionic strength [M]
  bjerrum               7.1         # Bjerrum length [Å]

  tabpot_dr2            1           # resolution for tabulated pair potential [Å2]
  tabpot_Umin           1e-6        # assume u_pair = 0  if u_pair < tabpot_Umin [kT]
  tabpot_Umax           .1          # calculate u_pair exact if u_pair > tabpot_Umax [kT]
```